Geochemistry Geophysics Geosystems G3

Article
Volume 13, Number 11
28 November 2012
Q11013, doi:10.1029/2012GC004337
ISSN: 1525-2027

Published by AGU and the Geochemical Society

Acoustics variability of air gun signals recorded at intermediate ranges within the Lau Basin

DelWayne R. Bohnenstiehl and Corey M. Scheip
Department of Marine, Earth and Atmospheric Sciences, North Carolina State University, Raleigh, North Carolina 27606, USA (drbohnen@ncsu.edu)

Haru Matsumoto and Robert P. Dziak
Hatfield Marine Science Center, Oregon State University and the National Oceanic and Atmospheric Administration, Newport, Oregon 97365, USA

[1] During January–February 2009, an active-source seismic survey was performed over the Eastern Lau Spreading Center in the Lau Back-Arc Basin (21°S, 176°S). Acoustic signals generated by the *R*/V *Langseth*'s 36-gun pneumatic source array were recorded within the deep sound channel at offsets of 29–416 km. The local ocean acoustic environment is everywhere bottom limited, with seafloor depths within the study domain ranging from ~1700–2800 m. Low-frequency (4–125 Hz) sound levels are monitored using root-mean-square, energy-flux-density and zero-to-peak measurement techniques. From these field data, transmission loss is found to exceed the predictions of a geometric spherical spreading model. At similar ranges, arrival amplitudes vary by up to 20 dB and durations vary by a factor of three to six. The depth of the seafloor beneath the air gun source exhibits a positive correlation with arrival duration and a negative correlation with range-corrected amplitude, explaining up to 30% of the observed variation in both parameters. The strength of this correlation, however, varies for stations lying at different azimuths, highlighting the importance of seafloor aspect and slope in the coupling of bottom-interacting acoustic energy into the sound channel. Range-dependent ray tracing shows that shots deployed over shallower seafloor are more likely to produce sound channel trapped signals that propagate with limited bottom interaction. This results in arrivals that are more impulsive, with shorter durations and higher amplitudes. Shots deployed in deeper water typically undergo a larger number of bounces and are characterized by more emergent, longer duration and smaller amplitude arrivals.

Components: 10,700 words, 15 figures, 2 tables.

Keywords: Lau Basin; acoustic propagation; air gunning; ocean noise; seismic exploration.

Index Terms: 0935 Exploration Geophysics: Seismic methods (3025, 7294); 4259 Oceanography: General: Ocean acoustics.

Received 10 July 2012; **Revised** 4 October 2012; **Accepted** 23 October 2012; **Published** 28 November 2012.

Bohnenstiehl, D. R., C. M. Scheip, H. Matsumoto, and R. P. Dziak (2012), Acoustics variability of air gun signals recorded at intermediate ranges within the Lau Basin, *Geochem. Geophys. Geosyst.*, *13*, Q11013, doi:10.1029/2012GC004337.

1. Introduction and Motivation

[2] In recent decades, noise in the ocean has increased significantly over historic levels. Anthropogenic activities, such as commercial shipping, drilling, military and civilian use of sonar, and hydrocarbon exploration are chiefly responsible for this increase, which includes both ambient and transient acoustic inputs [*Andrew et al.*, 2002; *National Research*

Council, 2003; *Hildebrand*, 2004; *McDonald et al.*, 2006]. Scientists, policy makers and the general public have become increasingly concerned about increasing levels of ocean noise and the potential ecological impact for marine mammals and other organisms [*National Research Council*, 2003]. The concern is broad in scope, as both continuous (e.g., commercial shipping) and transient (e.g., seismic air gunning) sources may inhibit a marine species' ability to continue life-sustaining activities such as communicating, feeding, breeding and navigation [*Richardson et al.*, 1995; *Madsen et al.*, 2002; *National Research Council*, 2003; *Hildebrand*, 2004, 2005; *Madsen et al.*, 2006; *Soto et al.*, 2006; *Parks et al.*, 2007; *Southall et al.*, 2007].

[3] *Andrew et al.* [2002] and *McDonald et al.* [2006] have independently shown 10–12 dB increases in ambient ocean noise within the frequency band of 20–80 Hz and 30–50 Hz, respectively, off the western coast of the United States within the past three to four decades. This is consistent with the near doubling in the number of ships and the general increase in propulsion power (speed) and vessel size over the same time period [*Chapman and Price*, 2011]. Evidence that these acoustic changes are impacting the communications of some cetacean species is mounting. For example, *Parks et al.* [2007] document an increase in the start frequencies of Atlantic Right Whale upcalls since the mid-20th century, which they attribute to an increase in 5–200 Hz noise levels. In the mid-latitude Pacific, *Holt et al.* [2009] has shown that Killer Whales exhibit the Lombard effect, an involuntary increase in vocal amplitude within a nosier environment, resulting in an increased energetic cost to individuals.

[4] While increasing ambient noise levels may have significant ecological impacts, high intensity transient signals also threaten marine animals, and in rare cases may be associated with physical injury [*Richardson et al.*, 1995; *National Research Council*, 2003]. Perhaps the most well-known example is the link of mid-frequency naval sonar to mass strandings of Cuvier's beaked whales [*National Research Council*, 2003]. Behavioral changes, however, are more common than physical injury. In field experiments, surfacing, respiratory and diving changes in baleen whales have been observed at received levels above 142 dB re 1μPa and active avoidance observed at received levels above 152 dB re 1μPa [*Ljungblad et al.*, 1988; *Richardson et al.*, 1995].

[5] In recent years, increasing environmental concern and regulation has been leveed specifically at seismic surveying operations [e.g., *Malakoff*, 2002; *D'Spain et al.*, 2006], which generate transient acoustic energy using an array of pneumatic air guns. These activities are aimed at imaging the geology of the sub-seafloor environment, primarily in support of hydrocarbon exploration. Even though the duty cycle of the air gun source array is only 0.3%, *Hildebrand* [2004] estimates that on an annual basis, the acoustic energy introduced into the oceans by these surveys rivals the combined contribution of military sonars and the global fleet of super tankers. Moreover, due to their dominantly low frequency spectrum (≤100–200 Hz), air gun signals are transmitted efficiently within the deep ocean and have been detected at ranges exceeding 3000 km [*Blackman et al.*, 2004; *Nieukirk et al.*, 2004, 2012].

[6] As underwater sounds propagate through the oceans, the signals become delayed, distorted and weakened [*Urick et al.*, 1983]. Being able to quantify this signal degradation increases the accuracy of sound level predictions and allows for improved environmental impact assessment and mitigation. In addition, many applications of marine geophysics such as seismic and volcanic monitoring [*Fox et al.*, 1995], enforcement of a comprehensive nuclear test ban [*de Groot-Hedlin and Orcutt*, 2001b] and undersea communications rely heavily on understanding range- and path-dependent signal propagation.

[7] During the period 27 January through 24 February 2009 (~28 days or ~675 h), the R/V *Marcus G. Langseth* carried out an active-source seismic refraction survey along a ~100 km section the Eastern Lau Spreading Center, near 20°S, 175°W [*Dunn and Martinez*, 2011]. The survey produced approximately 9400 acoustic shots with an average time separation of 210 s. The acoustic source consisted of 36 air guns fired simultaneously at a depth of 9 m below the sea surface. An array of autonomous underwater hydrophones (AUH), part of a separate though concurrent project, recorded the seismic survey at distances of 29–416 km (Figure 1). These receivers were calibrated omni-directional sensors sampling at 250 Hz and moored at a depth of 1000 m within the basin's deep sound channel. Although a total of eight instruments were deployed during the survey, two sensors are excluded from our analysis due to problems with their pre-amplifier, which introduced unwanted noise into the analysis frequency band. Four of these remaining stations are part of a small aperture diamond-shaped array (~2 km separation between moorings), known as the M3 quad; these hydrophones will be treated as a single station unless otherwise noted.

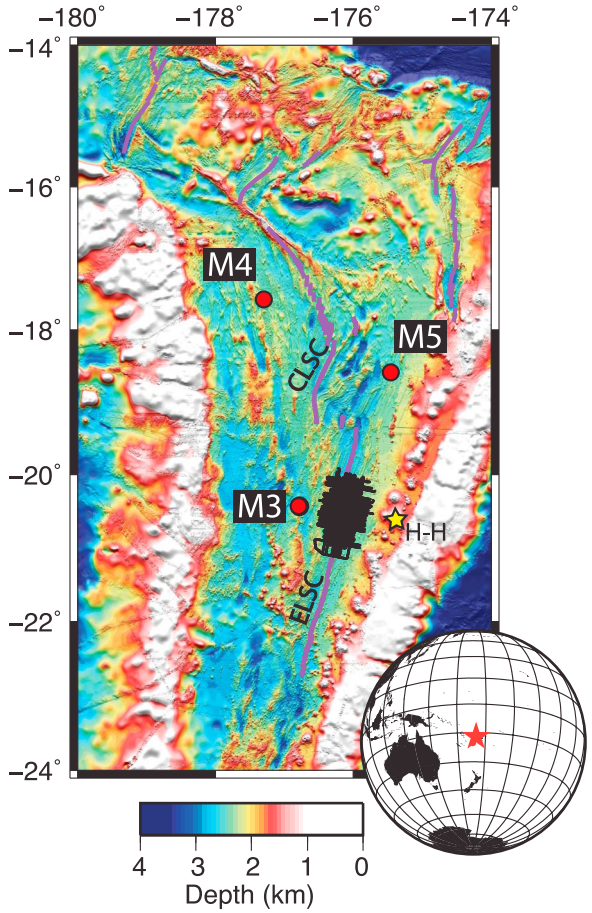

Figure 1. Bathymetric map of Lau Basin. Red circles denote locations of moored autonomous underwater hydrophones, black line shows seismic survey track and purple lines are spreading center traces. ELSC = Eastern Lau Spreading Center and CLSC = Central Lau Spreading Center. Yellow star indicates the site of the March 2009 eruption of Hunga-Ha'apai (H-H) volcano. Bathymetric data compilation courtesy of F. Martinez.

[8] Previous studies have addressed the propagation of anthropogenic air gun signals at short ranges, up to several kilometers [*Greene and Richardson*, 1988; *Tolstoy et al.*, 2004, 2009; *DeRuiter et al.*, 2006; *Madsen et al.*, 2002, 2006; *Breitzke et al.*, 2008; *Breitzke and Bohlen*, 2010; *Diebold et al.*, 2010], and long ranges, on the order of thousands of kilometers across ocean basins [*Blackman et al.*, 2004; *Nieukirk et al.*, 2004]. Despite the potential for behavior impacts [e.g., *Malakoff*, 2002; *Risch et al.*, 2012; *Castellote et al.*, 2012], few field studies have investigated transient air gun noise levels at the intermediate ranges studied here. Our objectives are to empirically quantify range-dependent signal characteristics and transmission loss within the Lau Basin and identify factors influencing the variability in the signal amplitude and duration at a given range. Although Blue, Humpback, Bryde's and Fin whales may be present within the basin [*Brodie and Dunn*, 2011], our study is not aimed at assessing the ecological impacts on specific local species.

2. Geo-acoustic Environment

[9] The active source survey of *Dunn and Martinez* [2011] was located along the central portion of Eastern Lau Spreading Center (ELSC), one of several back-arc spreading centers within the Lau Basin (Figure 1). At the latitude of the survey (20–21°S), the local spreading rate is ~65 mm/yr, and the ELSC topography transitions from a narrow axial high (south) to a broad, faulted axial valley (north) [*Taylor et al.*, 1996; *Martinez et al.*, 2006] (Figure 2). Side-scan sonar imagery shows high amplitude acoustic backscatter along the axis of the rift, consistent with the presence of a thinly sedimented basaltic basement [*Martinez et al.*, 2006]. Sonar backscatter strength decreases as sediment thickness increases off-axis, with volcano-clastic turbidites and nano-fossilliferous clays ponding within local fault-bounded basins [*Hawkins*, 1995]. To the east, the Tongan volcanic arc supplies clastic sediments that form a westward-thinning apron.

[10] The ocean acoustic environment of the tropical Lau Basin is everywhere bottom limited, meaning that the critical depth of the sound channel, at ~5500 m depth, lies well below the relatively shallow (1700–2800 m) depth of the seafloor (Figure 3a). For an air gun source near the sea surface, even rays with subhorizontal departure angles are refracted downward and intersect the seafloor. For a flat-lying seafloor, these rays are reflected and return to the sea surface, where they are reflected again, repeating the process (Figure 3b).

[11] For more realistic bathymetry (e.g., Figure 3c), some of these bottom-interacting rays may become entrapped in the SOund Fixing And Ranging (SOFAR) channel [*Ewing and Worzel*, 1948], where they propagate with minimal transmission loss for very long distances [*Tolstoy and Ewing*, 1950; *Urick et al.*, 1983]. The most commonly proposed mechanisms for SOFAR entrapment are downslope conversion [*Johnson et al.*, 1963] and seafloor scattering [*de Groot-Hedlin and Orcutt*, 1999, 2001a; *Park et al.*, 2001]. These mechanisms operate concurrently and are not mutually exclusive.

[12] Downslope conversion is a mechanism through which the grazing angles of acoustic rays are

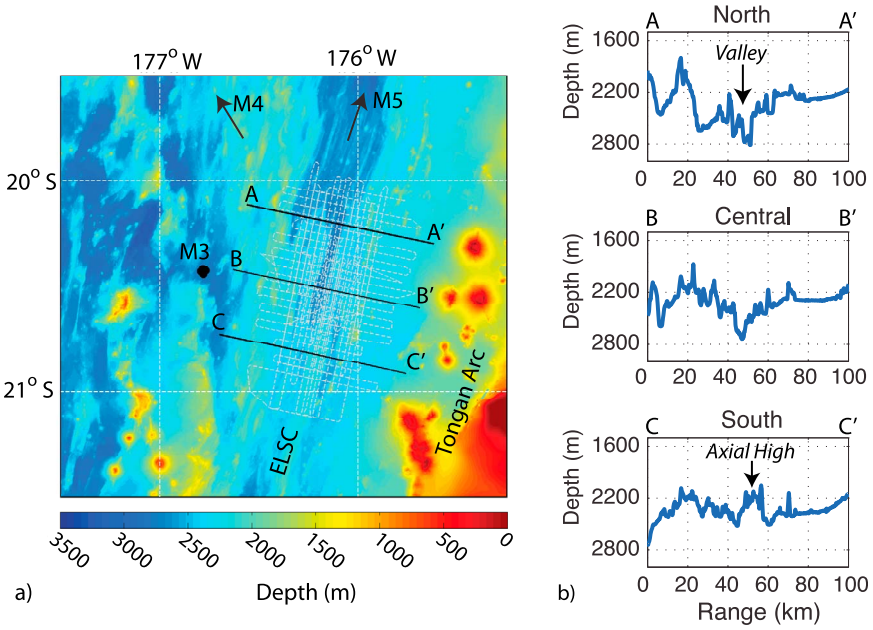

Figure 2. (a) A bathymetric map of the seismic survey (gray dashed line) area. (b) Three depth profiles crossing the ELSC are extracted, highlighting a deepening rift valley to the north and a transition to axial high morphology in the south.

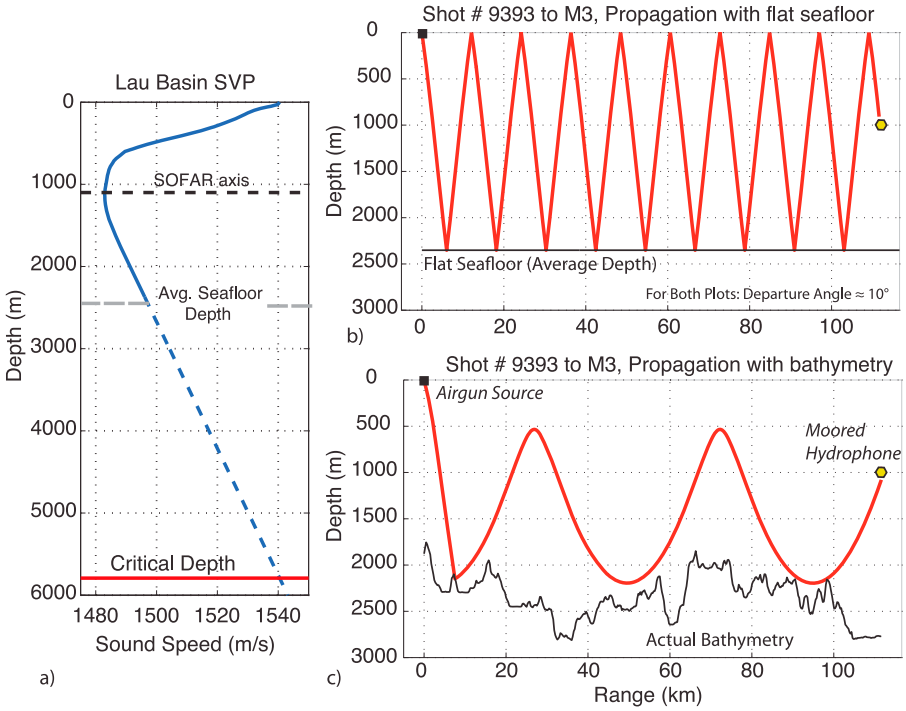

Figure 3. (a) Sound velocity profile (SVP) of the Lau Basin. The sound speed at 20.5°S, 176° W is taken from the January–March average data within the World Ocean Atlas [*Antonov et al.*, 2006, *Locarnini et al.*, 2006]. This profile is representative of the larger survey domain. The SOFAR axis depth is ~1100 m (black dashed line), the average depth is 2360 m (gray dashed line) and the critical depth of the sound channel is ~5500 m (red solid line). (b) Sub-horizontal, low grazing angle rays (<10°) emitted from a shallow source show that a flat seafloor will result in bottom and sea surface reflected propagation along the entire path. (c) Replacing flat seafloor with sloping bathymetry can cause a ray emitted at a similar grazing angle to become entrapped in the low-velocity zone and follow a continuously refracting path. The air gun source position is depicted with a black square and the moored hydrophone position by a yellow haxagon.

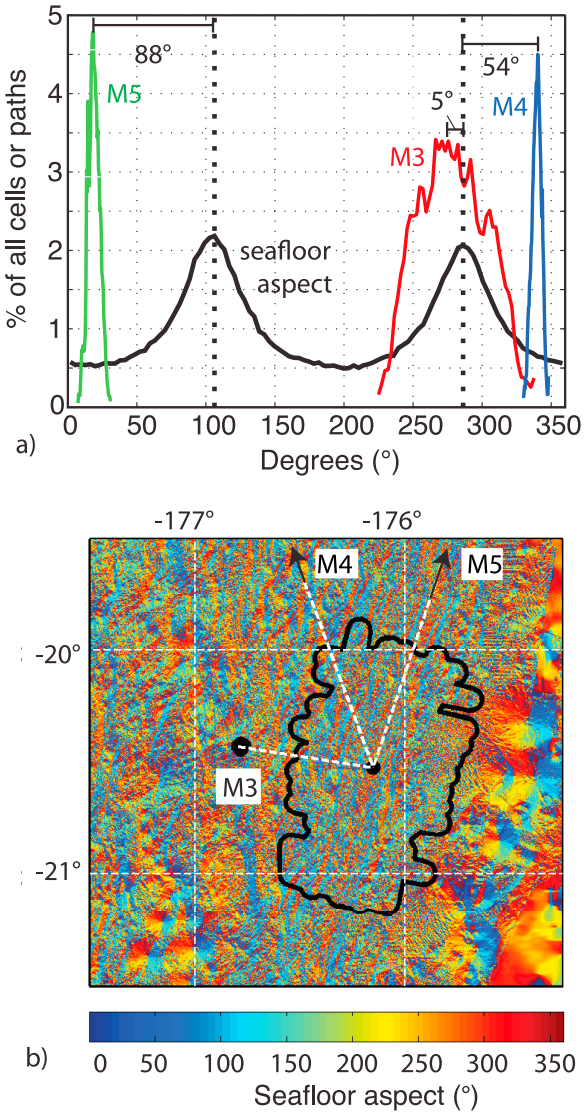

Figure 4. (a) The azimuths from the shot locations to each hydrophone (colored lines) are compared to the seafloor aspect directions in the study site (black line). (b) Aspect map showing alternating 100° and 280° facing topography associated with abyssal faulting adjacent to the spreading axis. Black line delineates survey area; black circle denotes M3 location and arrows point toward M4 and M5.

progressively decreased through a series of reflections off of a downward sloping seafloor, eventually leading to the entrapment of some rays in the low velocity sound channel [*Johnson et al.*, 1963; *Talandier and Okal*, 1998]. It is called upon most commonly to explain the coupling of seismo-acoustic energy into the water column across continental and island shelves, where long and continuous slopes exist; however, for the sloped and facetted seafloor associated with an oceanic rift, some specular reflections may become entrapped after only one or two seafloor bounces (Figure 3c).

[13] Due to the roughness and heterogeneity of the sea bottom, acoustic energy also is scattered back into the water column [*Bradley and Stephen*, 1996; *Park et al.*, 2001]. For sub-seafloor (earthquake) sources this is often described using a normal mode representation. In this view, low order modes, which are equivalent to low-grazing-angle rays, represent acoustic energy trapped in the SOFAR channel with minimal seafloor interaction. Neglecting variability in seabed parameters, scattering at shallower seafloor depths preferentially excites these low order modes; whereas higher order modes, which interact more strongly with the seafloor, are excited with increasing seafloor depths [*de Groot-Hedlin and Orcutt*, 1999, 2001a; *Park et al.*, 2001].

[14] The geometry of the Lau Basin AUH array is such that each receiver lies in a different azimuthal direction from the seismic survey, promoting variable seafloor interactions along the propagation paths (Figure 1). Seafloor aspects (slope directions) cluster around 100° and 280°, representing the inward and outward dipping normal fault scarps associated with the north trending ELSC (Figure 4). The M3 quad lies to the west of the ELSC on ~2 Ma crust; it records signals that propagate at azimuths between 225 and 338°, sub-parallel to the dominant seafloor aspect direction. Station M4 lies to the northwest of the air gun survey, and acoustic paths to this station (azimuths of ~340°) must cross the ELSC and Central Lau Spreading Center (CLSC), as well as some shallow seamounts. Signals received at station M5 propagate at azimuths of ~18°, traveling parallel to the seafloor fabric and rift valley (Figure 4). The seafloor deepens with range between the ELSC and the M3 quad station, with an average of 889.7 ± 120.8 m of relief along the propagation path. The M4 and M5 station are moored above seafloor of nearly the same depth; however, the average relief along the propagation paths is 940.9 ± 102.1 m and 694.5 ± 145.0 m, respectively. These path dependent bathymetries contribute to variability in recorded signal properties–as demonstrated empirically in this study.

[15] The complex tectonics of the Lau Basin create a naturally noisy acoustic environment, with active seismo-acoustic sources associated with the subduction interface and slab, the many shallow submarine volcanoes within the arc, and the ridge-transform system within the back arc [*Conder and Wiens*, 2011]. There were 22 seismic events with a magnitude of >4.2 during the 28-day time period of the R/V

Langseth survey (International Seismological Centre, on-line bulletin, Thatcham, U. K., 2001, http://www.isc.ac.uk), and ongoing analysis of the hydroacoustic records has located several thousand smaller earthquakes and volcano-acoustic signals that occurred during this period. For the purposes of this study, these natural signals are considered noise. Section 3.3 describes the procedures used to carefully identify and exclude air gun arrivals containing coincident volcanic and seismic energy.

3. Methods

3.1. Data Sources and Acquisition

[16] All of the AUH sensors sampled at 250 Hz and recorded continuously throughout the R/V *Langseth*'s active source seismic survey in January and February of 2009, capturing a total of 28197 arrivals (9399 shots × 3 stations). The receivers recorded changes in acoustic pressure with a 16-bit A/D resolution and signals were not clipped during the experiment. The frequency-dependent system response of the AUH's is removed before processing. A fifth-order 4 Hz high-pass Butterworth filter is applied to all data to filter out low-frequency ocean noise, some seismo-volcanic activities, and possible cable strumming noise. The effective bandwidth for the analysis is 4–125 Hz.

[17] The R/V *Langseth*'s 36-gun source array consists of four 16-m long strings (sub-arrays) towed with a nominal horizontal separation of 6–8 m. Each string contains nine active air guns and one ready spare [*Tolstoy et al.*, 2009]. Individual air gun source volumes range from 60 to 360 in^3, with a total volume of 6600 in^3. Air gun arrays are designed to generate a downward directed pulse of acoustic energy; for some arrays, the gun geometry and overall dimensions also can lead to horizontal directivity. The horizontal directivity of the R/V *Langseth*'s four-string 36-gun array was investigated in detail during the vessel's acoustic calibration cruises in 2007 and 2008 [*Tolstoy et al.*, 2009]. Using direct and short-offset arrivals acquired over flat-bottom sites within the Gulf of Mexico, *Tolstoy et al.* [2009] found no correlation between the broadband (5–25,000 Hz) signal amplitude and the ship's heading. They concluded that the R/V *Langseth*'s four-string 36-gun array behaves as a symmetrical broadband source at horizontal ranges greater than ~300 m [see *Tolstoy et al.*, 2009, Figures 10 and 11].

3.2. Signal Characteristics

[18] *Dunn and Martinez* [2011] provided the air gun shot locations and times from cruise MGL0903. From these meta-data, arrival times were estimated at each of the AUH recorders, assuming a constant sound speed of 1490 m/s. For each arrival, a 30 s data window centered on the predicted arrival time is extracted from the waveform database. In keeping with other air gun propagation studies [*Madsen et al.*, 2006; *Tolstoy et al.*, 2009; *Diebold et al.*, 2010], a cumulative energy method is used to select the 90% energy window and determine the duration of each arrival. This involves generating a cumulative sum of the squared amplitudes across the initial 30-s data window, and selecting the start and stop times of the arrival packet as the points encompassing 5% and 95% of the energy in the signal.

[19] Studies focused on air gun arrivals at shorter offsets (100–1000 s m) [e.g., *Madsen et al.*, 2006; *Tolstoy et al.*, 2009; *Diebold et al.*, 2010] typically use much shorter (~1 s) windows of integration; however, at the ranges studies here, within the bottom-limited acoustic environment of the Lau Basin, significant energy is found in the arrival coda at later times. We conducted comparisons using initial integration windows between 15 and 60 s in length. Integrating over too short a time window produces arrival durations that are clearly clustered near the half-window length—indicating that significant energy in the arrival coda is not being captured. On the other hand, integrating over too long a time window only serves to introduce unwanted transient volcano-seismic noise into the analysis. We therefore selected the shortest time window (30 s) for which the arrival durations stabilized at all three stations.

[20] Three methods are used to report received sound levels, as measured over the determined 90% energy windows. The values in decibels are calculated as follows:

$$\text{Root-mean-square:}\quad dB_{RMS} = 20 \cdot \log_{10}\left(\left(\frac{1}{n}\sum_{i=l}^{n}(s_i - \bar{s})^2\right)^{\frac{1}{2}}\right) \cdot [\text{re}\,1\mu\text{Pa}] \tag{1}$$

$$\text{Energy flux-density:}\quad dB_{EFD} = dB_{RMS} + 10 \cdot \log_{10}(d) \cdot [\text{re}1\mu\text{Pa}^2 \cdot \text{s}] \tag{2}$$

$$\text{Zero-to-Peak:}\quad dB_{Z2P} = 20 \cdot \log_{10}\{\max(|s|)\} \cdot [\text{re}1\mu\text{Pa}] \tag{3}$$

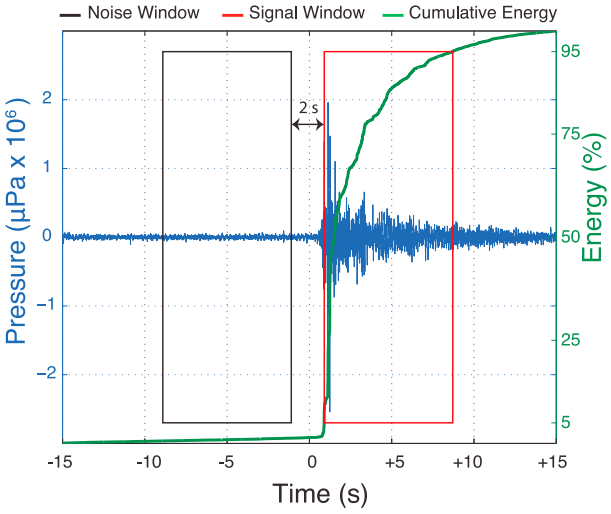

Figure 5. Waveform of shot 8000 received at station M4 (range = 330 km) overlain by cumulative energy sum plot (green). (right) The red window represents the 90% energy window used for signal level calculation (time between 5% and 95% of total cumulative energy). (left) The black window is a window of equal length situated such that it ends two seconds before the signal window begins; this is used for noise level calculations.

where s is the response-corrected pressure time series (μPa) and d is the duration in seconds of the n-point analysis window capturing 90% of the signal energy.

[21] The root-mean-square pressure (RMS) of the signal is the standard measure used in ambient (continuous) noise monitoring studies. The use of this measurement in describing transient sound sources is problematic in that the RMS level is sensitive to the choice of arrival window [*Madsen*, 2005]. Despite this limitation, the U.S. National Marine Fisheries Service (NMFS) has adopted RMS criteria for permitting and regulating active source seismic surveys. The received levels presently defined as safety criteria (intended to avoid risk of auditory impairment or injury) are 190 and 180 dB_{RMS} for pinnipeds and cetaceans, respectively, with 160 dB_{RMS} identified as the level above which there is likely to be behavioral disturbance [*Southall et al.*, 2007].

[22] The energy flux density (EFD) of the signal is proportional to the energy per unit area [*Young*, 1970] and the sound exposure level for a plane wave propagating in an unbounded medium [*Madsen*, 2005]. It is defined as the linear product of the square of the RMS amplitude and the duration of the arrival packet. Although current NMFS regulations do not utilize this measure, EFD is arguably a robust indicator of exposure due to a correction factor for signal duration (equation (2)), and it is increasingly cited in acoustic monitoring and conservation studies [e.g., *Madsen* 2005, *Tolstoy et al.* 2009; *Diebold et al.*, 2010].

[23] Zero-to-peak pressure (Z2P) is a measure of the maximum signal amplitude within the arrival packet and is commonly used to report sound levels of impulsive (transient) signals. For an aperiodic wave, Z2P levels are often higher than RMS values by 15 dB or more [*Madsen*, 2005].

[24] For each signal, a noise window is selected having the same duration as the arrival window (Figure 5). This window is positioned to end two seconds prior to the onset of the arrival window, as determined by the 90% cumulative energy approach. Signal-to-noise ratios (SNR) at each station are approximately normally distributed with significantly different means for the M3 quad (27.5 ± 5.6 dB), M4 (13.7 ± 6.7 dB) and M5 (18.5 ± 5.4 dB) stations (Figure 6). As background noise levels are shown to be within a few dB of each other (see section 4), this largely reflects the different ranges at which the signals are recorded, with M4 being positioned approximately five times further from the air gun survey relative to the M3 quad.

3.3. Arrival Data Selection

[25] Both signal-to-noise ratios and cumulative energy goodness-of-fit criteria are used to rid the data set of arrivals contaminated by coincident volcanic and seismic signals. For each station, arrivals

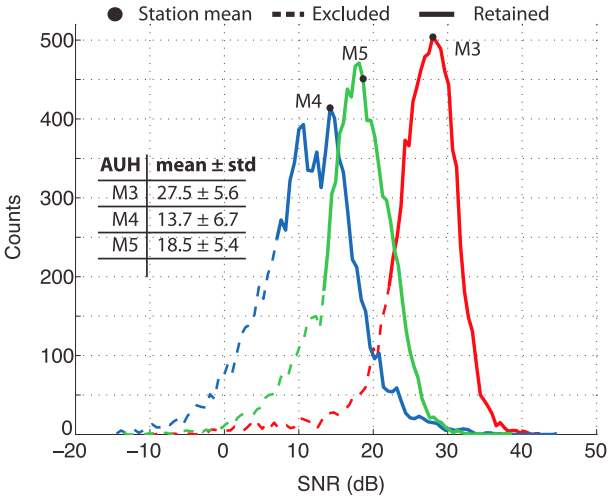

Figure 6. SNR distribution for each station. Dashed portions of each curve represent values where $SNR < \overline{SNR} - 1\sigma$. Arrivals with SNR in this range are not used for analysis. The average SNR is shown by a black dot along the histogram and the inset table provides summary statistics for each station.

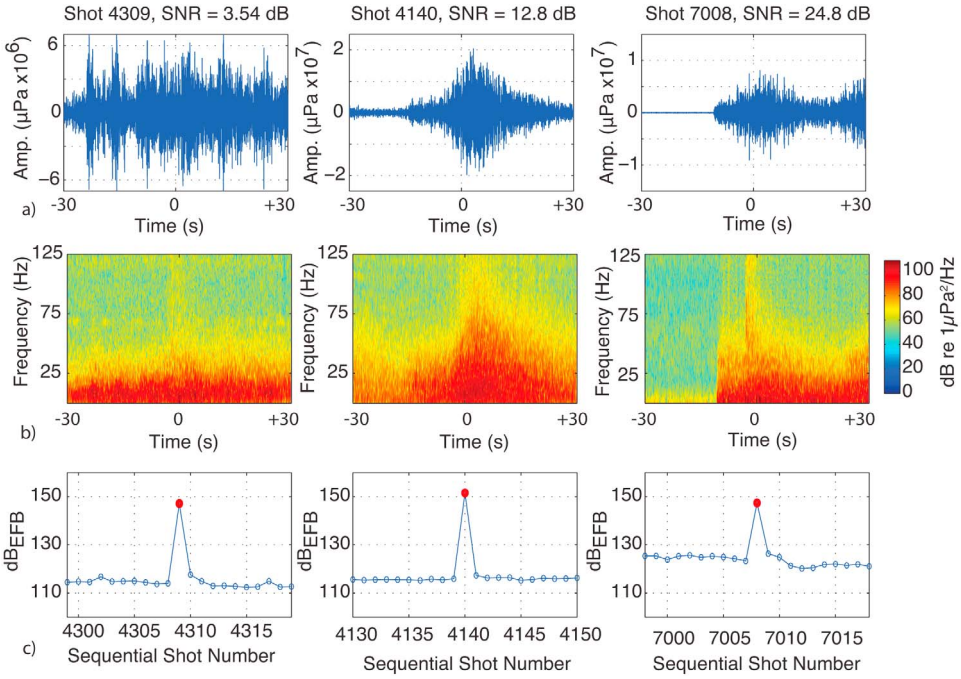

Figure 7. (a) Waveform and (b) spectrogram of shot numbers 4309, 4140 and 7008 (shown in columns) arriving at station M4. The signals are arranged with the predicted arrival time shown as t = 0. Coincident seismo-acoustic arrivals may result in low (4309), average (4140) or high (7008) SNR. Spectrograms are calculated within 0.5 s windows with 50% overlap. (c) Received levels (dB_{EFD}) are plotted for arrivals from successive shots. This illustrates the anomalously nature of the depicted arrivals (red dots), relative to those associated with shots immediate before and after (blue dots) that lie at a similar ranges and undertake similar propagation paths. Only the arrival associate with shot 4309 would be eliminated based on the SNR threshold, indicating that this criterion alone is not sufficient to eliminate air gun arrivals contaminated by transient seismo-volcanic energy.

with a SNR less than $\overline{SNR} - 1\sigma$ are excluded from the analysis (Figure 6). This removes 5835 arrivals (21%) from the total of 28197. However, given the extremely high rate of transient signal arrivals associated with seismic and volcanic activity within the basin and arc, there are many 'contaminated' arrivals that exhibit acceptable or even elevated SNR's. Such signals (Figure 7) are not removed by this criterion.

[26] Integrating the broadband signal energy (squared-amplitudes) over the original 30-s data window, which is centered on the predicted arrival time, reveals that suspect arrivals with acceptable SNR's typically exhibit a cumulative envelope shape that deviates from the expected pattern (Figures 5 and 8). A simple goodness-of-fit test is established, whereby signals are accepted only if their cumulative energy is below 5% at t = −1 s and above 35% at t = +5 s (Figure 8). These threshold values were chosen based on the average trend of all cumulative sum curves among all hydrophones. They are set to eliminate the ~20% of the remaining arrivals with the most anomalous cumulative sum shapes.

[27] Applying the SNR and goodness-of-fit criteria leaves a data set of 17491 arrivals for analysis—an extremely large data set compared with other air gun field studies [cf. *Blackman et al.*, 2004; *Tolstoy et al.*, 2004, 2009]. The number of rejected arrivals from individual hydrophones varied, with 1900 arrivals removed from M3, 5799 removed from M4 and 3007 removed from M5. A total of 2398 shots had arrivals that passed to all three stations. Using the accepted arrivals at each station, the associated noise window measurements are averaged to estimate the ambient noise floor during the survey.

3.4. Estimation of Transmission Loss

[28] A principal motivation in calculating acoustic received levels (RL) at varying ranges (R) is the determination of the transmission loss (TL), or the change in sound level relative to a reference distance (R_o) of one meter:

$$TL = |x| \log_{10}(R/R_o) \quad [\text{dB re 1m}] \tag{4}$$

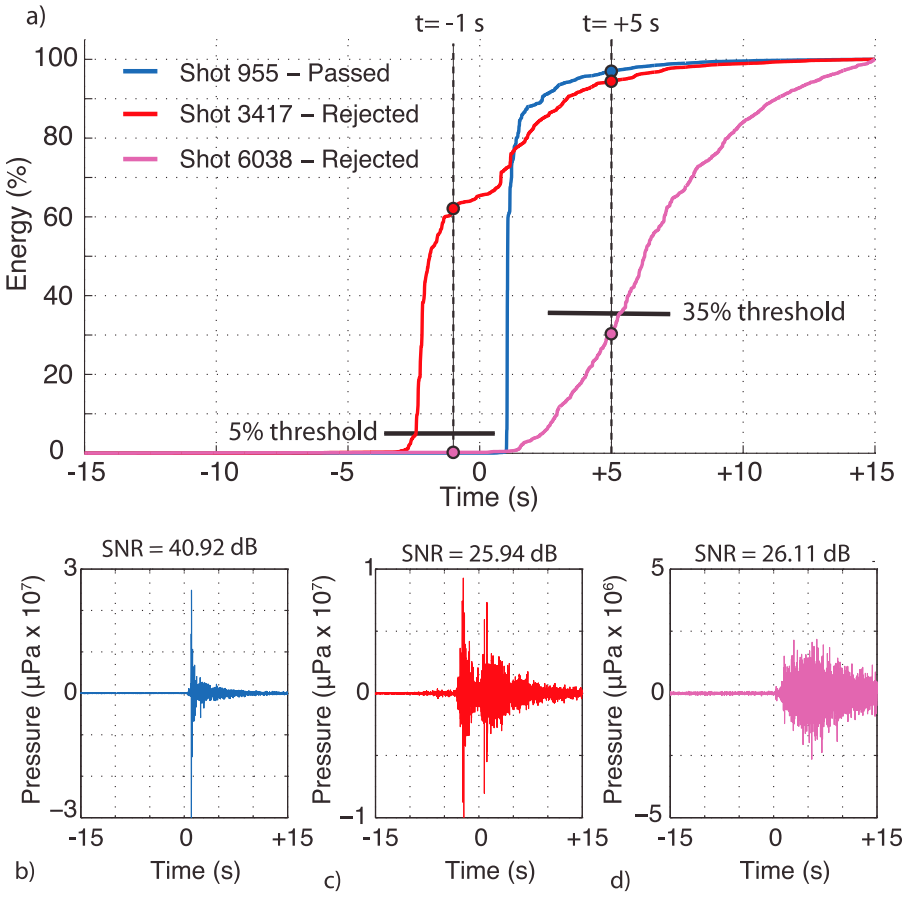

Figure 8. (a) Cumulative energy versus time plot for three arrivals with high SNR received at the M3 hydrophone. The data are positioned such that t = 0 s represents the predicted arrival time. (b) Shot 955 (blue) exhibits a cumulative-energy curve with abrupt onset and steadily decreasing coda amplitudes through time. This shape is typical for an air gun arrival at intermediate ranges, and the event is retained for analysis. From the inspection of the cumulative sum plots for all arrivals, a simple goodness-of-fit test is established, whereby signals containing more than 5% of their cumulative energy at t = −1 s or less than 35% of their cumulative energy at t = +5 s are eliminated due to possible contamination by transient seismic or volcanic noise. (c) Shot 3417 (red) fails this test. The cumulative energy reaches ∼60% at t = −1 s and there appears to be a transient noise arriving just prior to the air gun arrival. (d) Shot 6038 (magenta) also fails this test, with only ∼30% of its cumulative energy arriving before t = +5 s. Such an anomalous arrival pattern is typically observed when unwanted seismo-acoustic energy arrives late in the arrival analysis window.

where the TL coefficient (x) represents the negative slope on a logarithmic plot of RL versus R. Common values for $|x|$ range from 10 (i.e., cylindrical spreading) to 20 (i.e., spherical spreading) [*Urick et al.*, 1983]. In the bottom-limited Lau Basin, a value higher than 20 is expected because of scattering and reflection loss, which are not accounted for in geometrical spreading models [*Jensen et al.*, 1995]. To estimate the source level of the air gun array—a measure of the signal amplitude corrected to an offset of one meter—the decibel TL (equation (4)) is summed with the decibel RL (equations (1)–(3)):

$$SL = TL + RL \quad [\text{dB @ 1 m}] \tag{5}$$

[29] The decibel RL versus $\log_{10}(R)$ data are regressed in a least squares sense, with the slope of the best fit line indicating the TL coefficient (equation (4)) and the y-intercept providing an estimate of the acoustic source level (Figure 9). Due to the closely spaced nature of elements within the M3 quad (∼2 km between individual instruments), the four sensors are averaged both for range and received level to avoid giving greater weight to these short-offset arrivals. The resulting parameters are summarized in Table 1. Unless otherwise noted, reported uncertainties in TL and SL represent the standard error in the slope and intercept as determined using a standard bootstrap procedure (n = 5000). As is

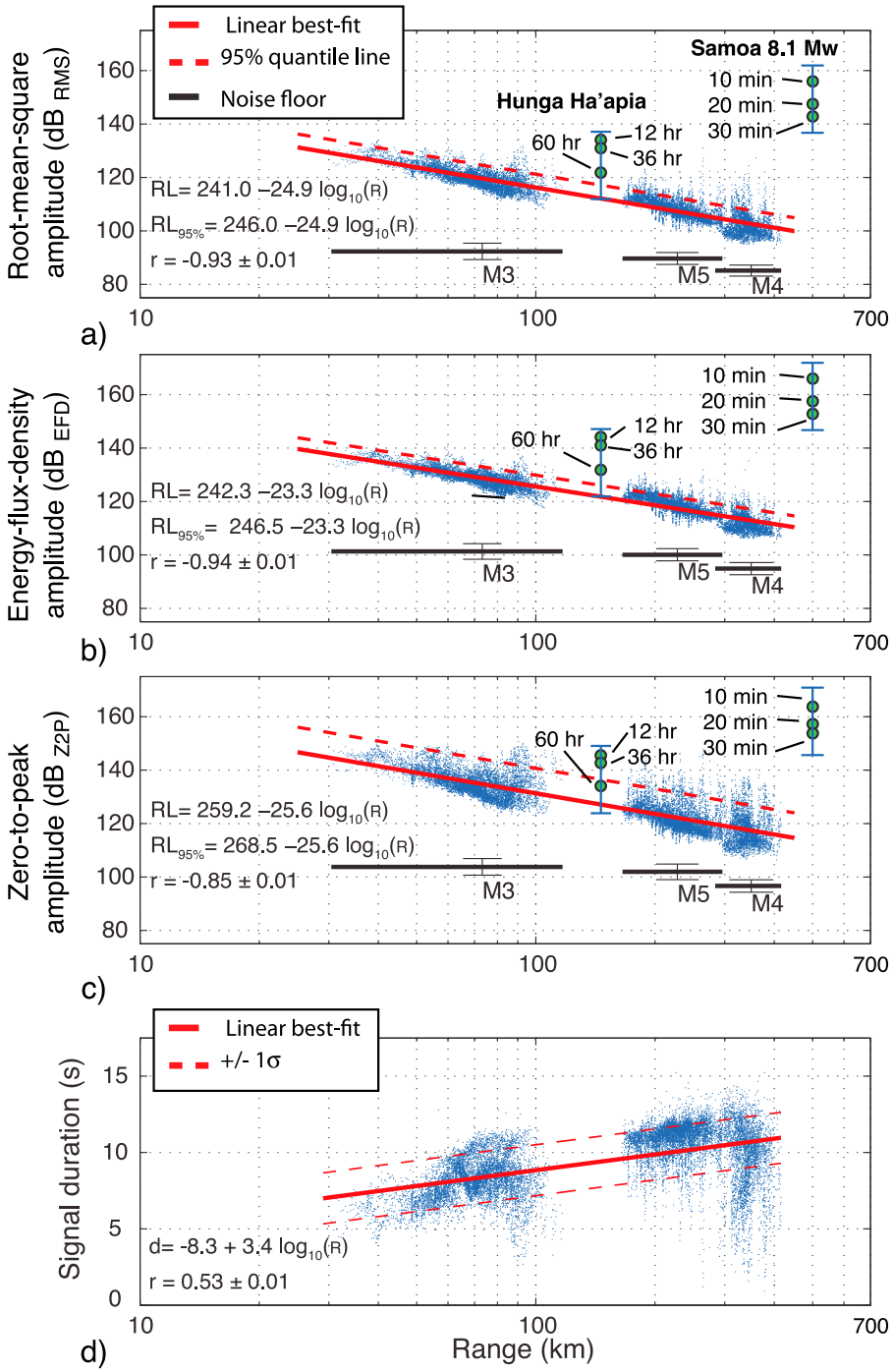

Figure 9. Received levels (dB) as a function of range are reported as (a) RMS, (b) EFD and (c) Z2P values. A least squares best fit line is plotted (red) as well as a quantile line (dashed red) indicating the level for which 95% of the data fall below. Black lines represent the ambient noise floor for each hydrophone station; error bars indicate $\pm 1\sigma$. Also shown are the median received amplitudes (estimated for a series of 10-s duration arrival windows) recorded during the March 2009 eruption of Hunga Ha'apai volcano (station M3) and following the great Samoa M_w 8.1 earthquake in September of 2009 (station M5). Median values are shown for different observation periods, as labeled (green dots). See Table 2. (d) 90% cumulative energy arrival durations are plotted a function of range. The best fit prediction is shown (solid red line) with $\pm 1\sigma$ confidence limits (dashed red line). In-line and cross-line shots occupy the same amplitude range and are therefore regressed together. This finding is consistent with the horizontally symmetrical nature of the R/V *Langseth*'s four-string 36-gun source reported during calibration [*Tolstoy et al.*, 2009].

Table 1. Transmission Loss Coefficients and R/V *Langseth* 36-Gun Array Source Levels

	This Study		*Tolstoy et al.* [2009][b]	
Measurement	Trans. Loss Coefficient[a]	SL Estimate dB ro. 1 m[a]	Trans. Loss Coefficient	SL Estimate dB ro. 1 m
RMS	24.9 ± 0.1	241.0 ± 0.4	29.21	260.45
EFD	23.3 ± 0.1	242.3 ± 0.3	32.34	258.98
Z2P	25.6 ± 0.1	259.2 ± 0.6	Not Reported	Not Reported

[a]Reported uncertainties represent the standard error in the slope and intercept based on 5000 bootstrap samples. Confidence intervals (1σ) [*Draper and Smith*, 1998, p. 82] for the prediction of SL (RL at a range of 1 m) are ±3.0, 2.5, and 4.7 dB for RMS, EFD and Z2P data sets, respectively.
[b]*Tolstoy et al.* [2009] results based on analysis of direct arrivals recorded at ranges 0.5–2.9 km; frequency band 5–25,000 Hz.

common in mitigation studies, a line defining the 95% quantile of the received level data also is defined parallel to this best fitting trend [e.g., *Tolstoy et al.*, 2009].

4. Results

[30] The recorded RMS sound levels vary from ~130 to 100 dB_{RMS} at ranges of 29 to 416 km, between ~28 and 15 dB above ambient noise levels. The transmission loss coefficient (|x|) is 24.9 ± 0.1 and the back-calculated source level is 241.0 ± 0.4 dB_{RMS} @ 1 m (Figure 9a). Across the measured ranges, the received levels plot within 3 dB of the best fit approximation with 1σ confidence, with the maximum spread in amplitude at a given offset (station M4 arrivals) spanning more than 15 dB.

[31] Arrival durations varied from 0.9 s to 15.2 s, with the mean and standard deviation at each station being 8.1 ± 1.4 (M3), 9.6 ± 2.3 (M4) and 10.9 ± 1.1 (M5) seconds. Since nearly all of the arrival durations exceed one second, EFD sound levels will typically exceed their RMS equivalents (equation (2)). When the EFD data are fit, the transmission loss coefficient is found to be 23.3 ± 0.1 and a back-calculated source level is 242.3 ± 0.3 dB_{EFD} @ 1 m. EFD received levels lie within 2.5 dB of the best fit line with 1σ confidence. The most extreme variation in received level at a similar range again occurs at the M4 station; however, the spread is reduced to ~10 dB (Figure 9b).

[32] Regression of the decibel Z2P versus $\log_{10}(R)$ data indicate a best fitting transmission loss coefficient of 25.6 ± 0.1 and an acoustic source level of 259.2 ± 0.6 dB_{Z2P} @ 1 m. The Z2P data exhibit higher variability than RMS and EFD measures, even at close offsets, with a 1σ confidence band of ±4.7 dB about the prediction and a >20 dB (a linear order of magnitude) spread in values at a given range (Figure 9c).

5. Discussion

5.1. Sound Levels and Transmission Loss

[33] Regardless of the method used to characterize sound levels, the observed transmission loss exceeds $20 \cdot \log_{10}(R)$ (i.e., spherical spreading loss) (Figures 9a–9c and Table 1). These high coefficients result from the strongly bottom-limited acoustic environment and the shallowness of the source, which leads to significant interaction with the ocean-atmosphere and ocean-seafloor boundaries [*Jensen et al.*, 1995; *Urick et al.*, 1983] (Figure 3). The back-calculated sources levels estimated in the present study are ~17–20 dB lower than values reported for a deep site (1700 m) in the Gulf of Mexico during the R/V *Langseth*'s calibration cruises (Table 1) [*Tolstoy et al.*, 2009]. These measurements, however, may not be directly comparable, since *Tolstoy et al.* [2009] considered only direct arrivals at ranges of 500 to 2900 m, and monitored sound levels over a broader 5–25,000 Hz frequency band.

[34] Even at the nearest ranges studied here, sound levels fall short of United States Level B harassment thresholds (160 dB_{RMS}) and the142 dB_{RMS} level where disruptions in diving patterns have been observed among some cetacean populations [*Ljungblad et al.*, 1988; *Richardson et al.*, 1995; *Southall et al.*, 2007]. Recent studies, however, have cites changes in baleen whale call patterns associated with fisheries sonars (~415 Hz) and air gun activity for signal levels of only ~20 dB_{rms} above ambient [*Castellote et al.*, 2012; *Risch et al.*, 2012]. Such levels are met at nearly all ranges monitored in this study (Figure 9), and the frequency content of the air gun source is within the zone of audibility for baleen whales and other marine species.

Table 2. Received Signal Levels Associated With Major Submarine Geophysical Events

Duration	Root-Mean-Square (dB_{RMS})	Energy-Flux-Density (dB_{EFD})	Zero-to-Peak (dB_{Z2P})
	March 2009 Hunga Ha'apai Eruption Recorded at M3		
	{25% 50%, 75%} Quantiles From 10 s Duration Arrival Windows		
	Observational Period Begins at 2009-03-16 16:00:00		
12 h	{131.9, 134.1, 137.1}	{141.9, 144.1, 147.1}	{143.0, 145.5, 150.0}
36 h	{124.5, 131.0, 134.2}	{134.5, 141.0, 144.2}	{136.8, 142.7, 146.2}
60 h	{111.9, 121.8, 132.2}	{121.9, 131.8, 142.2}	{122.9, 134.1, 143.9}
Air gun R = 146 km	112.1 ± 3.0[a]	121.8 ± 2.5[a]	127.1 ± 4.7[a]
	September 2009 Samoa Earthquake M_w 8.1 Recorded at M5		
	{25% 50%, 75%} Quantiles From 10 s Duration Arrival Windows		
	Observational Period Begins at 2009-09-29 17:49:00		
10 min	{152.9, 155.9, 160.0}	{162.9, 165.9, 170.0}	{161.0, 163.7, 167.7}
20 min	{140.4, 147.5, 155.9}	{150.4, 157.5, 165.9}	{151.3, 157.2, 163.7}
30 min	{138.6, 142.8, 153.0}	{148.6, 152.8, 163.0}	{148.8, 153.8, 161.1}
Air gun R = 500 km	98.8 ± 3.0[a]	109 ± 2.5[a]	113.4 ± 4.7[a]

[a]Mean values from best fitting regression $\pm 1\sigma$ confidence intervals [*Draper and Smith*, 1998, p. 82] for the prediction of RL at the given range.

[35] To gain some perspective on the contribution of the survey to the local noise budget, the acoustic energy is estimated from the EFD [*Hildebrand*, 2004, 2005]. Assuming the EFD back-calculated source level of 242 ± 0.3 dB_{EFD} @ 1 m, a water density of 1025 kg/m^3 and an average sound speed of 1490 m/s, 3.3×10^{10} J (±6.8%) of acoustic energy were released during the one-month-duration survey. Compared to other anthropogenic sources, this is approximately equivalent to 50 supertankers transiting for 30 days (100% duty cycle) or a military SURTASS LFA sonar operating for 6 days (10% duty cycle). Both of these sources operate at similarly low frequencies to air guns, typically ≤300 Hz [*Hildebrand*, 2004].

[36] Within such a volcanically and tectonically active basin, however, sustained periods of similarly high intensity sound generated from natural sources are not uncommon. For example, during 16–20 March 2009, the seamount Hunga Ha'apai erupted semi-continuously with a volcanic explosivity index (VEI) of 2 [*Vaughan and Webley*, 2010; *Bohnenstiehl et al.*, 2012]. It produced a repeating series of phreomagmatic explosions at a range of 146 km from M3. Starting at the onset of the eruption, received level information is calculated at M3 within a series of non-overlapping 10-s duration arrival windows, spanning observational periods of 12, 36 and 60 h after the start of the activity. The 25%, 50% and 75% quantile levels observed within these arrival windows are summarized in Table 2. During the first 12 h of the eruption, for example, median recorded sound levels are 134.1 dB_{RMS}, 144.1 dB_{EFD} and 145.5 dB_{Z2P}. These values can be compared to the predicted arrival levels of 112.1 dB_{RMS}, 121.8 dB_{EFD} and 127.1 dB_{Z2P} that would be recorded only intermittently at this range during the operation of the R/V *Langseth*'s 36-gun seismic array (Figure 9 and Table 2).

[37] Another example is the M_w 8.1 tsunamigenic earthquake that occurred along the outer rise of the Tonga trench on 29 September 2009 at a distance of 500 km from station M5. This event spawned two nearly coseismic Mw 7.8 sub-events along the Tonga subduction zone and a wide zone of aftershock activity across the upper plate [*Lay et al.*, 2010]. Acoustic received levels are calculated at station M5 over observational periods of 10, 20 and 30 min, capturing the main shock events and their immediate aftershocks (Table 2 and Figure 9). During the first 10 min following the initial acoustic arrivals, median recorded sound levels are 155.9 dB_{RMS}, 165.9 dB_{EFD} and 163.7 dB_{Z2P}. These values can be compared to the predicted arrival levels of 98.8 dB_{RMS}, 109.3 dB_{EFD} and 113.4 dB_{Z2P} that would be recorded only intermittently if the R/V *Langseth*'s 36-gun array were discharged at a range of 500 km (Figure 9 and Table 2).

[38] Based on the recorded signal levels and applying our empirical transmission loss relationship (Figure 9b), the Hunga eruption produced $\sim 3 \times 10^{13}$ J and the great Samoan earthquake produced $\sim 3 \times 10^{14}$ J of acoustic energy that were released into the water column. When compared to the entire seismic survey ($\sim 10^{10}$ J), the energy contributions of these geophysical events are 3–4 orders of magnitude higher. Notably, the lower energy release associated with the air gun survey also occurs over a significantly longer duration, ~675 h.

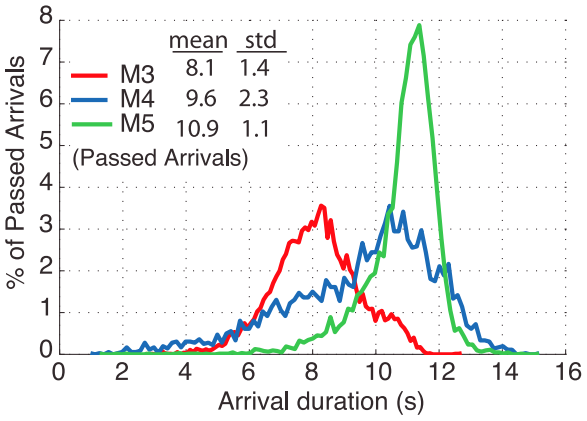

Figure 10. Histogram of arrival durations at each hydrophone. Inset table gives the mean and standard deviation of each population. Duration is defined using the 5–95% cumulative energy sum method. See section 3.2 for a description of methodology.

5.2. Signal Characteristics and Bathymetry

[39] This section investigates how signal characteristics are influence by the near-source bathymetry. Our approach involves 1) identifying arrivals with extreme (high and low) amplitudes and durations, and examining their spatial patterns with regard to the morphology of the ridge axis, and 2) quantifying the correlation between these arrival characteristics and the water depth directly beneath each shot.

[40] Arrival durations, as defined by the 90% cumulative energy window, generally increase with increasing source-receiver offset (Figures 9d and 10). Variability at a given range, however, is especially notable at stations M3 and M4, which exhibit greater bathymetric relief along their propagation paths, compared to station M5. When those shots with the longest and shortest durations (defined as above and below the best fit line $\pm$ 1σ) are plotted on a map of the seismic survey, a geographic trend becomes apparent (Figure 11a), whereby the short duration arrivals tend to originate above shallow topography and long duration arrivals tend to originate within the deeper valley. Similarly, arrivals with high and low peak amplitudes plot preferentially along the ridges and valleys, respectively (Figure 11b). Extreme RMS and EFD values follow a similar, though perhaps less pronounced pattern (Figures 11c and 11d).

[41] To further quantify this relationship, the depth of the seafloor beneath each shot is extracted from the 100-m horizontal resolution bathymetric grid derived from a compilation of shipboard swath data collected along the ELSC. Although air guns signals in this environment scatter and reflect sound from some area of the seafloor beneath the shotpoint, the depth directly beneath the shot is used as a simple proxy—keeping in mind the first-order persistence of abyssal seafloor depths [e.g., *Herzfeld et al.*, 1995]. Correlating these shot depths with the received signal durations and estimated source levels (decibels), the geographic trends identified in Figure 11 are confirmed. Signal duration and the Z2P decibel source level display a similar level of correlation with seafloor depth, explaining between 12 and 30% (|r| = 0.34–0.54) of the variance at the three stations (Figures 12a and 12b). RMS and EFD decibel source levels exhibit a somewhat weaker correlation with depth, |r| = 0.26–0.46 (Figure 12c) and |r| = 0.21–0.44 (Figure 12d), respectively. Correlation coefficients also show a pattern based on receiver station, with the durations measured at the M3 station and the source level estimates from station M4 being most strongly correlated with the depth of the seafloor beneath the shot. For each signal parameter, the data from station M5 shows the weakest correlation with seafloor depth (Figure 12).

[42] This study is not the first to present evidence linking seafloor depth and bathymetric properties with variability in acoustic received levels. *Blackman et al.* [2004] has shown that a receiving station thousands of kilometers away detected seismic air gun shots fired above a sloping seafloor near the Ninety East Ridge in the Indian Ocean, while that same receiver did not detect shots fired at closer ranges, but in deep water (>4000 m). Modeling results indicated that shots fired over the ridge typically coupled into the SOFAR channel by downslope conversion and increased the SNR proportionately [*Harben et al.*, 2002], while other shots relied on seafloor scattering from shallow secondary sources for SOFAR entrapment [*Blackman et al.*, 2004]. Observations from *Blackman et al.* [2004] and *Harben et al.* [2002] are consistent with the present study, where peak amplitudes and arrival durations can be correlated to seafloor parameters near the source array.

[43] The link between seafloor and received signal characteristics is further supported by the study of T-phases, which are hydroacoustic signals generated by the conversion of seismic P and S-waves at the ocean-crust boundary [*Tolstoy and Ewing*, 1950]. Ray tracing results of *Williams et al.* [2006], for example, indicate that T-phases emanating from deep seafloor entrain less energy into

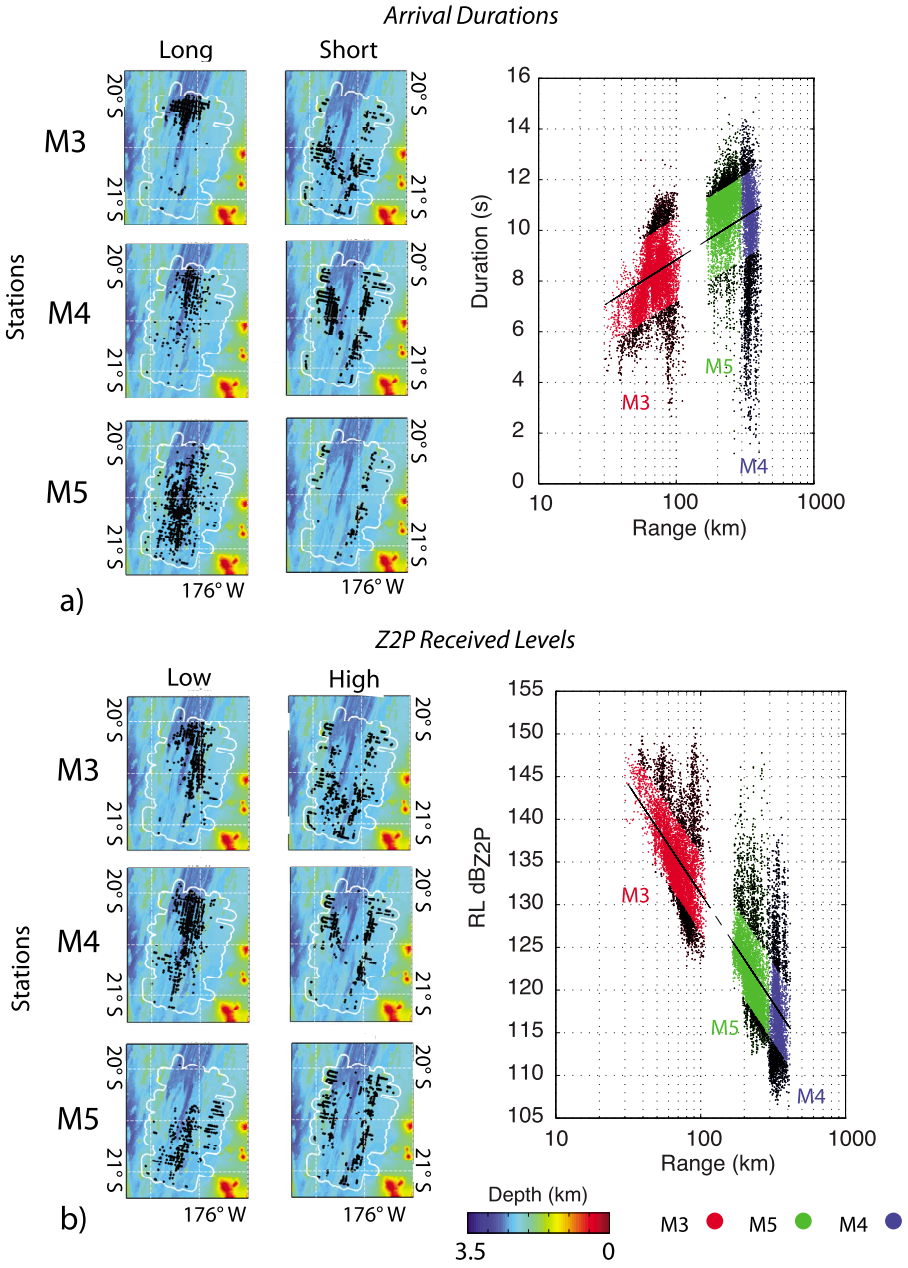

Figure 11. (a) Arrival duration, (b) Z2P, (c) RMS and (d) EFD received levels are plotted versus $\log_{10}(R)$ in the right hand column. Measurements deviating from the expected value (solid black line) by more than $\pm 1\sigma$ are defined as extreme (black dots) and plotted separately in map view on the lefthand side. White line on the maps delineates the limits of the air gun survey area. Arrivals (at a given range) with the shortest durations and highest amplitudes typically plot along bathymetric highs. The longest duration and lowest amplitude arrivals cluster along the deeper sections of the ELSC.

the SOFAR channel than those emanating from shallow seafloor.

5.3. Acoustic Propagation in a Bottom Limited Setting

[44] The sound velocity structure in the Lau Basin is such that the minimum velocity, and thus the SOFAR axis, is at a depth of ~1100 m and the critical depth is ~5500 m (Figure 3a). The air gun source is shallow (9 m) and consequently acoustic energy cannot be refracted directly into the SOFAR channel. Rather, signals scatter and specularly reflect from some area beneath the air gun array; this can generate low grazing angle rays (low order modes) that propagate over very long ranges [*Talandier and Okal*,

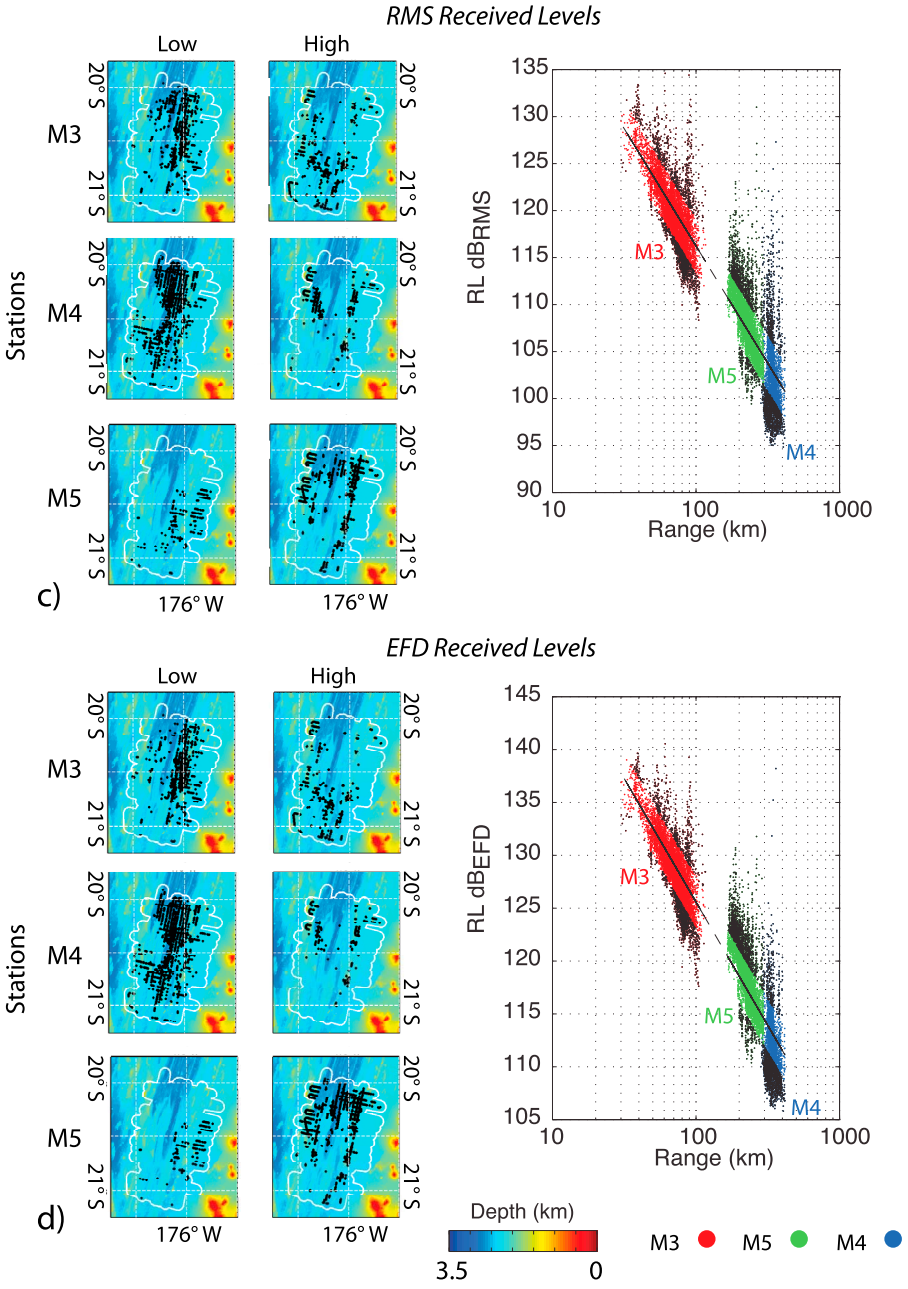

Figure 11. (continued)

1998; *Park et al.*, 2001]. Sites of seafloor scattering, which radiate energy both in and out of the propagation plane, may be viewed as secondary acoustic sources [*Yang and Forsyth*, 2003; *Williams et al.*, 2006]. The strength and directivity of this scattered acoustic energy depends on the ray's incident angle and the slope and aspect of the seafloor [*Blondel*, 2009].

[45] The influence of scattering from the rough and heterogeneous ELSC crust is evident in the arrival durations, which are an order of magnitude higher than the direct arrivals reported at ranges of up to a few kilometers from the R/V *Langseth*'s 36-gun array [*Tolstoy et al.*, 2009]. Bottom interaction leads to longer duration arrivals in the Lau Basin, and increasing the source-receiver offset increases the possibility of bottom interaction along the propagation path. This is evident by the increase in average arrival duration observed at the more distant stations M4 and M5, relative to station M3 (Figure 10).

[46] When propagation occurs via bottom-interaction, acoustic arrivals are expected to both loose energy

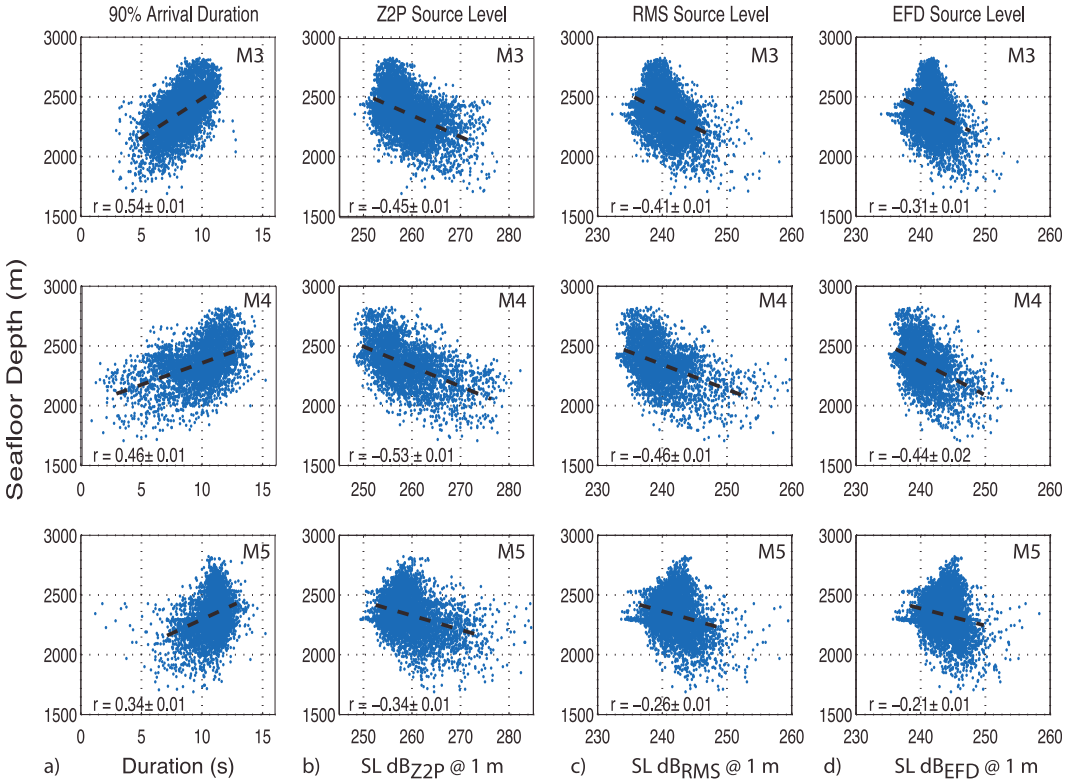

Figure 12. (a) Arrival duration and (b) Z2P, (c) RMS and (d) EFD source levels (range-corrected amplitudes) are plotted against the seafloor depth at the corresponding seismic shot locations. Black lines represent a linear best fit to the data. Arrival durations correlate positively with depth, whereas source levels correlate negatively with depth. Correlation coefficients are given in each panel, with standard error bootstrap uncertainties.

and spread out in time with each seafloor bounce. As such, back-calculated source levels, which remove the first-order range dependence from the amplitude data, show a strong negative correlation with arrival durations (Figure 13). RMS and Z2P source levels show the strongest correlation ($-0.90 < r < -0.70$) with arrival duration. EFD estimates, which incorporate duration into their measurements (equation (2)), show a slightly weaker correlation ($-0.82 < r < -0.56$) (Figure 13).

[47] The correlations between arrival characteristics and seafloor depth (Figure 12) and between signal duration and amplitude (Figure 13) are explored using the Bellhop ray-tracing model [*Porter and Liu*, 1994]. The results are summarized in Figure 14. For each arrival, a total of 3000 rays are used to model propagation over the range-dependent bathymetry between the source (z = 9 m) and receiver (z = 1000 m). The model also considers range-dependent sound speed profiles, extracted from the 2005 edition of the World Ocean Atlas [*Locarnini et al.*, 2006].

[48] To identify source-to-receiver paths that favor sound channel entrapment of the propagating acoustic energy, the ray(s) undergoing the fewest number of bottom-bounces is identified for each model run (Figure 14). This is similar to the ray counting approach used to identify favorable propagation paths in seismo-acoustic investigations [e.g., *Talandier and Okal*, 1998; *Williams et al.*, 2006]. The distribution of modeled shots with rays undergoing only a few bounces (1 for station M3, and ≤3 for the more distant stations M4 and M5) mirrors the distribution of arrivals characterized as having anomalously high amplitudes and/or short durations (Figure 15). Similarly, the distribution of modeled shots that propagate dominantly through a series of seafloor reflections is found to mirror the distribution of arrivals characterized as having anomalously low amplitudes and/or long durations (Figure 15). Due to uncertainty in the bathymetry and sound velocity data, as well as the limits imposed by considering only in-plane propagation and disregarding scattering in these models, this correlation is not one-for-one; however, the same first-order spatial patterns are evident in the observed (Figure 15a) and modeled (Figure 15b) panels.

[49] Although our discussion has focused on the importance of seafloor depth beneath the source

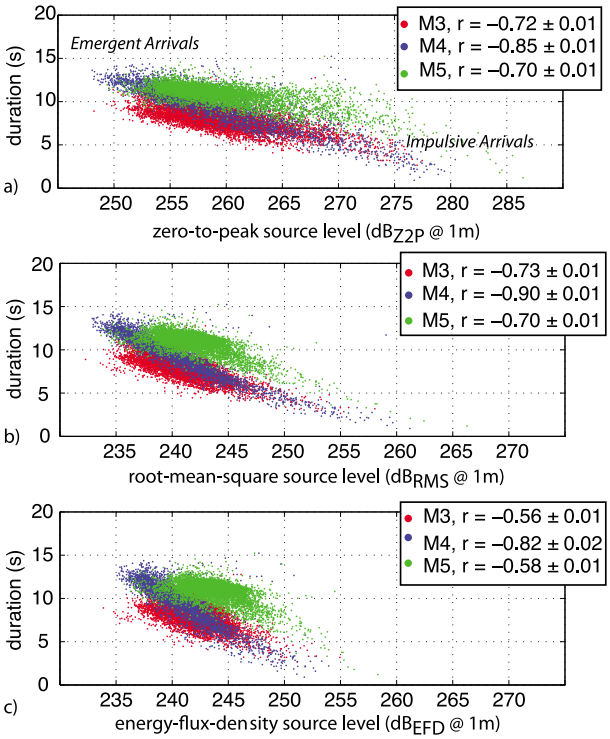

Figure 13. Arrival durations are plotted versus acoustic source level (range-corrected amplitude) measured in terms of the (a) zero-to-peak (Z2P), (b) root-mean-square (RMS) and (c) energy flux density (EFD). Z2P and RMS values show strongest correlations, whereas EFD shows the weakest correlation for all hydrophones. For each measurement technique, the signals recorded at station M4 exhibit the strongest correlation.

(Figure 12), the bathymetry along the propagation path also influences the observed signal characteristics. Consequently, the spatial patterns observed in Figure 15 are not identical for the each station. This path dependence also influences the correlations discussed earlier. Station M5, for example, lies to the north of the ELSC rift valley such that source-receiver paths tend to shallow or stay relatively flat (Figure 4). Consequently, signal characteristics observed at M5 shows the least correlation with the depth of water beneath the source (Figure 12). The arrival durations observed at station M5 also exhibit the smallest standard deviation (Figure 10), likely reflecting the less variable nature of bathymetry along profiles trending parallel to the seafloor fabric [e.g., *Herzfeld*, 1993].

[50] Different sound level measures (equations (1)–(3)) show similar trends, but exhibit different levels of correlation (Figures 12 and 13). The Z2P measurement is concerned with the largest instantaneous pressure recorded at any point within the arrival window. When the acoustic source level (range-corrected amplitude) is expressed in these terms, the estimates show the largest spread in value, and correlate strongly with the signal duration (Figure 13a) and the depth of the seafloor (Figure 12b). The RMS measurements represent the signal amplitude average across the arrival window. When used to define the acoustic source level, these values show less total variation, a similar level of correlations in terms of arrival duration and a somewhat weaker correlation with seafloor depth (Figures 12a and 13c). The EFD amplitude, which incorporates arrival duration, is often described as a measure of the sound exposure level. When this parameter is used to define the source level, the returned values show the least variability and the weakest correlations with arrival duration and seafloor depth (Figures 12d and 13c). EFD source level estimates therefore provide the most consistent measure of the air gun array's source strength in this bottom-limited environment.

6. Summary

[51] During January–February 2009, an active-source seismic survey was performed over the Eastern Lau Spreading Center in the Lau Backarc Basin (21°S, 176°S). Acoustic signals generated by the R/V *Marcus G. Langseth*'s 36-gun pneumatic source array were recorded within the deep sound channel at offsets of 29–416 km. The local acoustic environment is everywhere bottom limited and transmission loss is found to exceed the predictions of a geometric spherical spreading model, with loss coefficients >20 dB/log$_{10}$(R).

[52] Due to the high degree of acoustic bottom interaction within this shallow, low-latitude basin, peak amplitudes at a given range vary as much as an order of magnitude and durations by a factor of three to six. Moreover, up to 30% of the variance in duration and range-corrected (decibel) amplitude is explained by a correlation with the water depth beneath the shot. A spatial pattern is identified that shows short-duration, high-amplitude, impulsive arrivals originate preferentially over shallow bathymetry; and, longer-duration, lower-amplitude, emergent arrivals originate preferentially over areas of deeper seafloor. These patterns are explored using a numerical ray trace model, which predicts that signals originating over shallow bathymetry are more likely to become entrapped within the sound channel; whereas, signals originating in deeper water are more likely to propagate via a repeating series of bottom reflections.

[53] In comparing Z2P, RMS and EFD measurements of signal amplitude, EFD measurements

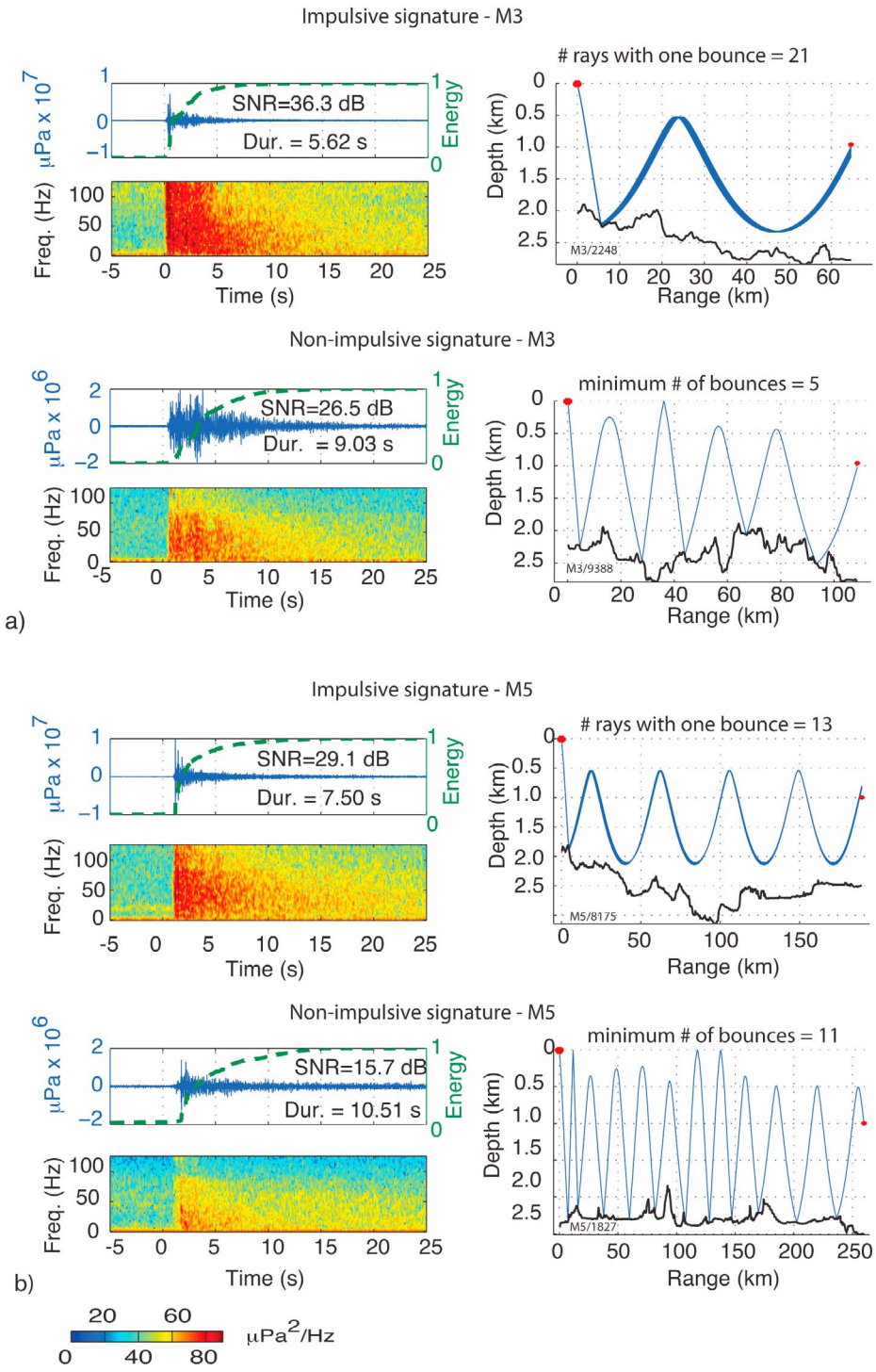

Figure 14. Sample air gun arrivals record at stations (a) M3, (b) M5 and (c) M4 (two examples). For each arrival, the pressure waveform (blue), cumulative energy curve (green) and spectrogram are shown. These examples illustrate the variable characteristics of the arrivals, with both impulsive, short-duration, higher-amplitude signals and more emergent, longer-duration, lower-amplitude signals observed for shots at similar ranges. For each shot, a range-dependent acoustic ray-tracing model [*Porter and Liu*, 1994] is performed using 3000 rays with take off angles evenly distributed between ±89°. Only those rays with the smallest number of bottom bounces are shown. Impulsive waveforms are associated with propagation paths that allow rays to become trapped in the sound channel after a small number of bottom bounces; more emergent waveforms are typically associated with signals that propagate laterally through a series of bottom reflections.

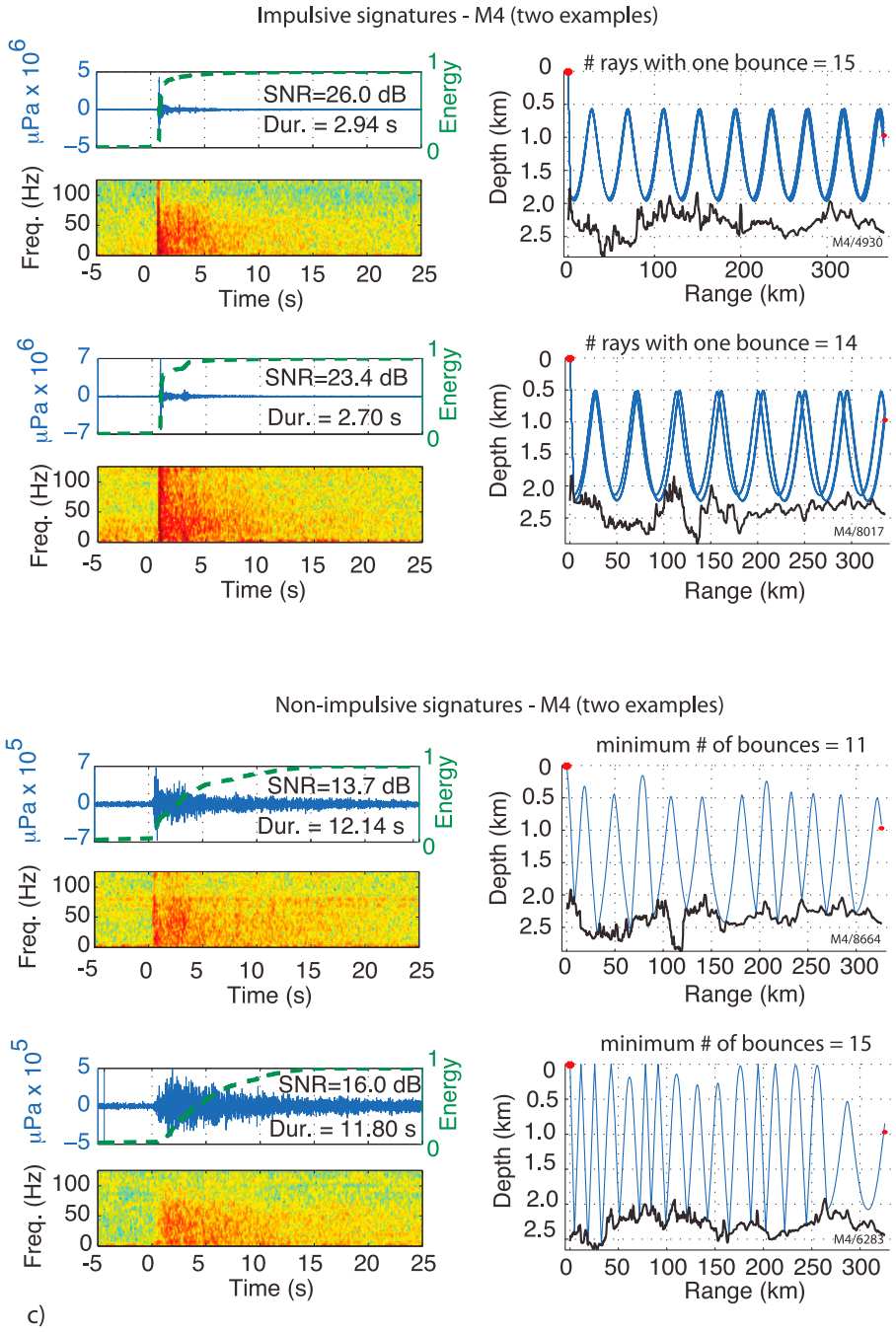

Figure 14. (continued)

correlate the least strongly with seafloor depth. This suggests that, in areas exhibiting significant bathymetric relief, this technique may provide a more robust estimate of the acoustic source level. EFD has become a common measure of exposure level in bioacoustics, and its reduced sensitivity to bathymetric-propagation effects argues that it should be considered more broadly as a tool in quantifying the size of transient geophysical signals.

[54] Although the R/V *Langseth*'s 2009 active source survey represented a significant anthropogenic input into the ocean soundscape of the Lau Basin, long-term acoustic monitoring suggests that the resulting transient sound levels are not uncommon within this

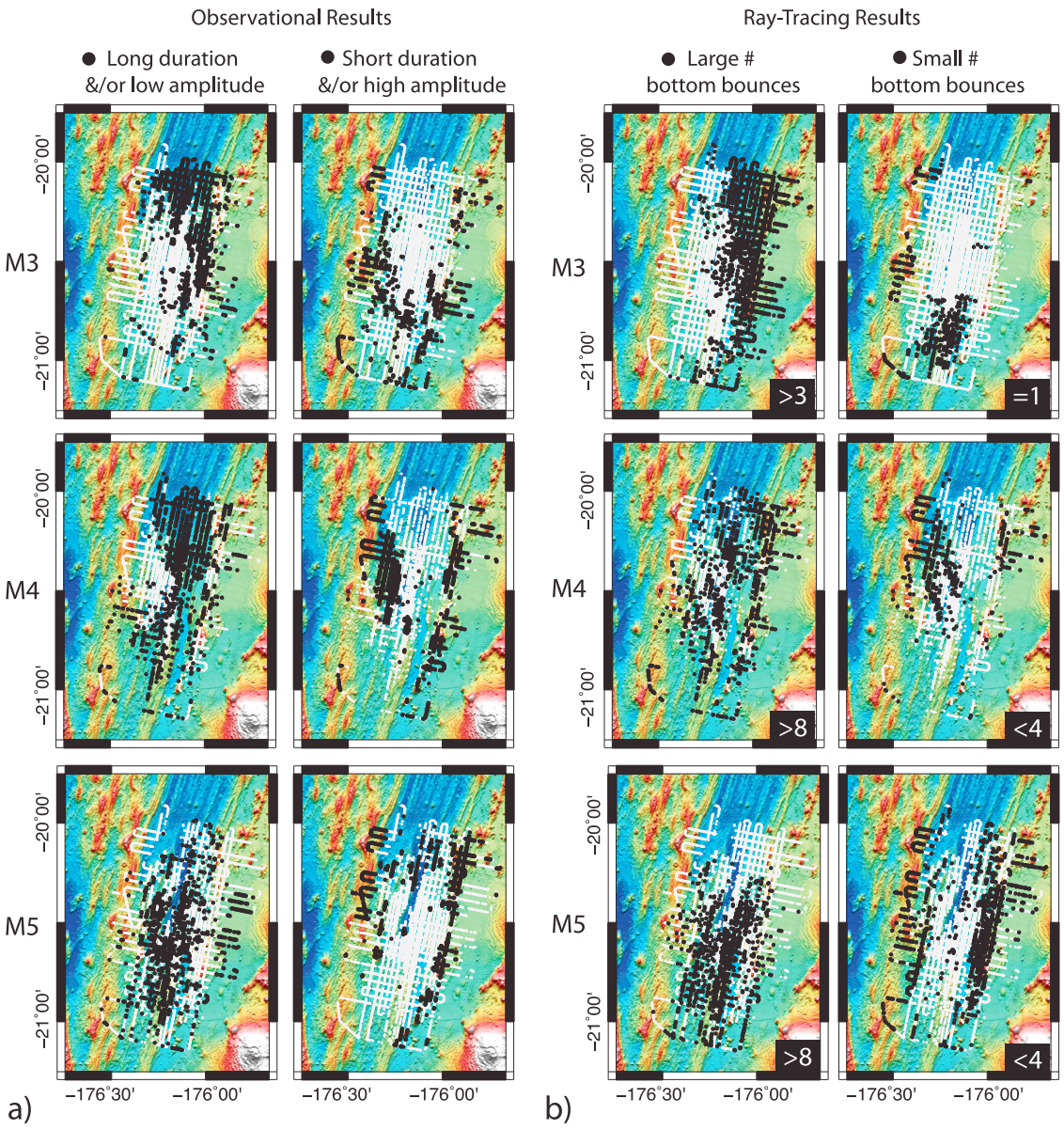

Figure 15. (a) The geographic distribution of air gun shots (black dots) producing arrivals with (left) extremely long duration and/or low amplitude signals and (right) short duration and/or high amplitude signals. These classifications are based on arrivals that lie more than $\pm 1\sigma$ from the predicted value at a given range (Figure 11). Shot-receiver pairs retained for analysis are shown as white dots. (b) Geographic distribution of shot locations modeled as having relatively (left) many or (right) few bottom-bounces (black dots). The number of bottom bounces used for classification is shown in the lower right of each map. All modeled shotpoints are shown as white dots.

extremely active tectonic and volcanic area. For example, the moderate (VEI = 2) eruption of Hunga Ha'apai volcano in March of 2009 [*Vaughan and Webley*, 2010; *Bohnenstiehl et al.*, 2012] produced sustained pressure levels that exceeded the air gun signals by more than 20 dB_{RMS} at a given range and released on the order of 1000 times more acoustic energy. The degree to which marine animals in this area have become habituated, or respond, to this naturally noisy low-frequency soundscape is unknown.

Acknowledgments

[55] We thank the captain and crew of the R/V *Marcus G. Langseth*, R/V *Roger Revelle* and R/V *Kilo Moana.* Critical to the success of this project were field technicians J. Shanley

(NOAA) and M. Fowler (NOAA/OSU), who oversaw the mooring deployment and recovery efforts, and NCSU graduate students J. Bowman, K. Cook, P. Monigle, J. O'Connor and K. Warren. Andy Lau provided vital assistance with software development and data quality control. F. Martinez provided access to his compilation of multibeam bathymetry within the basin, and R. Dunn kindly provided shot meta-data information for his MGL cruise. Comments by the Associate Editor (R. Dunn) and two anonymous reviewers significantly improved the quality of this manuscript. D.R.B. also thanks M. Tolstoy and the late J. Diebold for numerous discussions regarding seismic array operations and acoustics. This is PMEL contribution 3983. Research supported by National Science Foundation grants OCE-0825295 and OCE-1029278.

References

Andrew, R. K., B. M. Howe, J. A. Mercer, and M. A. Dzieciuch (2002), Ocean ambient sound: Comparing the 1960s with the 1990s for a receiver off the California coast, *Acoust. Res. Lett. Online*, *3*, 65–70, doi:10.1121/1.1461915.

Antonov, J. I., R. A. Locarnini, T. P. Boyer, A. V. Mishonov, and H. E. Garcia (2006), *World Ocean Atlas 2005*, vol. 2, *Salinity*, *NOAA Atlas NESDIS*, vol. 62, edited by S. Levitus, 182pp., NOAA, Silver Spring, Md.

Blackman, D. K., C. de Groot-Hedlin, P. Harben, A. Sauter, and J. A. Orcutt (2004), Testing low/very low frequency acoustic sources for basin-wide propagation in the Indian Ocean, *J. Acoust. Soc. Am.*, *116*, 2057–2066, doi:10.1121/1.1786711.

Blondel, P. (2009), Acoustic signals and data acquisition, in *The Handbook of Sidescan Sonar*, Praxis, pp. 7–34, Chichester, U. K.

Bohnenstiehl, D. R., R. P. Dziak, H. Matsumoto, and T.-K. Lau (2012), Underwater acoustic records from the March 2009 eruption of Hunga Ha'apai–Hunga Tonga volcano in the Kingdom of Tonga, *J. Volcanol. Geotherm. Res.*, doi:10.1016/j.jvolgeores.2012.08.014, in press.

Bradley, C. R., and R. A. Stephen (1996), Modeling of seafloor wave propagation and acoustic scattering in 3-D heterogeneous media, *J. Acoust. Soc. Am.*, *100*, 225–236, doi:10.1121/1.415952.

Breitzke, M., and T. Bohlen (2010), Modeling sound propagation in the Southern Ocean to estimate the acoustic impact of seismic research surveys on marine mammals, *Geophys. J. Int.*, *181*(2), 818–846, doi:10.1111/j.1365-246X.2010.0451.x.

Breitzke, M., O. Boebel, S. El Naggar, W. Jokat, and B. Werner (2008), Broad-band calibration of marine seismic sources used by R/V *Polarstern* for academic research in polar regions, *Geophys. J. Int.*, *174*, 505–524, doi:10.1111/j.1365-246X.2008.03831.x.

Brodie, D., and R. Dunn (2011), Detection of baleen whales on an ocean-bottom seismometer array in the Lau Basin, Abstract S31D-2266 presented at 2011 Fall Meeting, AGU, San Francisco, Calif., 5–9 Dec.

Castellote, M., C. W. Clark, and M. O. Lammers (2012), Acoustic and behavioral changes by fin whales (*Balaenoptera physalus*) in response to shipping and airgun noise, *Biol. Conserv.*, *147*, 115–122, doi:10.1016/j.biocon.2011.12.021.

Chapman, N. R., and A. Price (2011), Low frequency deep ocean ambient noise trend in the Northeast Pacific Ocean, *J. Acoust. Soc. Am.*, *129*(5), EL161, doi:10.1121/1.3567084.

Conder, J. A., and D. A. Wiens (2011), Shallow seismicity and tectonics of the central and northern Lau Basin, *Earth Planet. Sci. Lett.*, *304*, 538–546, doi:10.1016/j.epsl.2011.02.032.

de Groot-Hedlin, C. D., and J. Orcutt (1999), Synthesis of earthquake-generated T-waves, *Geophys. Res. Lett.*, *26*, 1227–1230, doi:10.1029/1999GL900205.

de Groot-Hedlin, C., and J. Orcutt (2001a), Excitation of T-phases by seafloor scattering, *J. Acoust. Soc. Am.*, *109*, 1944–1954, doi:10.1121/1.1361057.

de Groot-Hedlin, C., and J. Orcutt (Eds.) (2001b), *Monitoring the Comprehensive Nuclear-Test-Ban Treaty: Hydroacoustics*, Birkhäuser-Verlag, Basel, Switzerland, doi:10.1007/978-3-0348-8270-5.

DeRuiter, S. L., P. L. Tyack, Y.-T. Lin, A. E. Newhall, J. F. Lynch, and P. J. O. Miller (2006), Modeling acoustic propagation of airgun array pulses recorded on tagged sperm whales (*Physeter macrocephalus*), *J. Acoust. Soc. Am.*, *120*, 4100, doi:10.1121/1.2359705.

Diebold, J. B., M. Tolstoy, L. Doermann, S. L. Nooner, S. C. Webb, and T. J. Crone (2010), R/V *Marcus G. Langseth* seismic source: Modeling and calibration, *Geochem. Geophys. Geosyst.*, *11*, Q12012, doi:10.1029/2010GC003216.

Draper, N. R., and H. Smith (1998), *Applied Regression Analysis*, 3rd ed., 706 pp., Wiley, New York.

D'Spain, G. L., A. D'Amico, and D. M. Fromm (2006), Properties of the underwater sound fields during some well documented beaked whale mass stranding events, *J. Cetacean Res. Manag.*, *7*, 223–238.

Dunn, R. A., and F. Martinez (2011), Contrasting crustal production and rapid mantle transitions beneath back-arc ridges, *Nature*, *469*, 198–202, doi:10.1038/nature09690.

Ewing, W. M., and J. L. Worzel (1948), Long-range sound transmission, *Mem. Geol. Soc. Am.*, *27*, 1–35.

Fox, C. G., W. E. Radford, R. P. Dziak, T. K. Lau, H. Matsumoto, and A. E. Schreiner (1995), Acoustic detection of a seafloor spreading episode on the Juan de Fuca Ridge using military hydrophone arrays, *Geophys. Res. Lett.*, *22*, 131–134, doi:10.1029/94GL02059.

Greene, C. R., Jr., and W. J. Richardson (1988), Characteristics of marine seismic survey sounds in the Beaufort Sea, *J. Acoust. Soc. Am.*, *83*, 2246–2254, doi:10.1121/1.396354.

Harben, P. E., C. de Groot-Hedlin, and D. Blackman (2002), Acoustic sources for blockage calibration of ocean basins: Results from the October 2001 Indian Ocean cruise, report, Natl. Nucl. Secur. Admin., Washington, D. C.

Hawkins, J. W. (1995), Evolution of the Lau Basin: Insights from ODP leg 135, in *Active Margins and Marginal Basins of the Western Pacific*, *Geophys. Monogr. Ser.*, vol. 88, edited by B. Taylor and J. Natland, pp. 125–173, AGU, Washington, D. C., doi:10.1029/GM088p0125.

Herzfeld, U. C. (1993), A method for seafloor classification using directional variograms, demonstrated for data from the western flank of the Mid-Atlantic Ridge, *Math. Geol.*, *25*, 901–924, doi:10.1007/BF00891050.

Herzfeld, U. C., I. I. Kim, and J. A. Orcutt (1995), Is the ocean floor a fractal?, *Math. Geol.*, *27*, 421–462, doi:10.1007/BF02084611.

Hildebrand, J. (2004), Sources of anthropogenic sound in the marine environment, paper presented at International Workshop: Policy on Sound and Marine Mammals, U.S. Mar. Mammal Comm. and Joint Nat. Conservation Comm., London.

Hildebrand, J. A. (2005), Impacts of anthropogenic sound, in *Marine Mammal Research: Conservation Beyond Crisis*, edited by J. E. Reynolds et al., pp. 101–124, John Hopkins Univ. Press, Baltimore, Md.

Holt, M. M., D. P. Noren, V. Veirs, C. K. Emmons, and S. Veirs (2009), Speaking up: Killer whales (*Orcinus orca*) increase their call amplitude in response to vessel noise, *J. Acoust. Soc. Am.*, *125*, EL27–EL32, doi:10.1121/1.3040028.

Jensen, F., W. A. Kuperman, M. B. Porter, and H. Schmidt (1995), *Computational Ocean Acoustics*, Springer-Verlag, New York.

Johnson, R. H., J. Northrop, and R. Eppley (1963), Sources of Pacific T-phases, *J. Geophys. Res.*, *68*, 4251–4260.

Lay, T., C. J. Ammon, H. Kanamori, L. Rivera, K. D. Koper, and A. R. Hutko (2010), The 2009 Samoa-Tonga great earthquake triggered doublet, *Nature*, *466*, 964–968, doi:10.1038/nature09214.

Ljungblad, D. K., B. Würsig, S. L. Swartz, and J. M. Keene (1988), Observations on the behavioral responses of bowhead whales (*Balaena mysticetus*) to active geophysical vessels in the Alaskan Beaufort Sea, *Arctic*, *41*, 183–194.

Locarnini, R. A., A. V. Mishonov, J. I. Antonov, T. P. Boyer, and H. E. Garcia (2006), *World Ocean Atlas 2005*, vol. 1, *Temperature*, NOAA Atlas NESDIS, vol. 61, edited by S. Levitus, 182 pp., NOAA, Silver Spring, Md.

Madsen, P. (2005), Marine mammals and noise: Problems with root mean square sound pressure levels for transients, *J. Acoust. Soc. Am.*, *117*, 3952–3957, doi:10.1121/1.1921508.

Madsen, P., B. Møhl, B. Nielsen, and M. Wahlberg (2002), Male sperm whale behaviour during exposures to distant seismic survey pulses, *Aquat. Mamm.*, *28*, 231–240.

Madsen, P. T., M. Johnson, P. Miller, N. A. Soto, J. Lynch, and P. Tyack (2006), Quantitative measures of air-gun pulses recorded on sperm whales (*Physeter macrocephalus*) using acoustic tags during controlled exposure experiments, *J. Acoust. Soc. Am.*, *120*, 2366–2379, doi:10.1121/1.2229287.

Malakoff, D. (2002), Suit ties whale deaths to research cruise, *Science*, *298*, 722–723, doi:10.1126/science.298.5594.722.

Martinez, F., B. Taylor, E. T. Baker, J. A. Resing, and S. L. Walker (2006), Opposing trends in crustal thickness and spreading rate along the back-arc Eastern Lau Spreading Center: Implications for controls on ridge morphology, faulting, and hydrothermal activity, *Earth Planet. Sci. Lett.*, *245*(3–4), 655–672, doi:10.1016/j.epsl.2006.03.049.

McDonald, M. A., J. A. Hildebrand, and S. M. Wiggins (2006), Increases in deep ocean ambient noise in the Northeast Pacific west of San Nicolas Island, California, *J. Acoust. Soc. Am.*, *120*, 711–718, doi:10.1121/1.2216565.

National Research Council (2003), *Ocean Noise and Marine Mammals*, Natl. Acad. Press, Washington, D. C.

Nieukirk, S. L., K. M. Stafford, D. K. Mellinger, R. P. Dziak, and C. G. Fox (2004), Low-frequency whale and seismic airgun sounds recorded in the mid-Atlantic Ocean, *J. Acoust. Soc. Am.*, *115*, 1832–1843, doi:10.1121/1.1675816.

Nieukirk, S. L., D. K. Mellinger, S. E. Moore, K. Klinck, R. P. Dziak, and J. Goslin (2012), Sounds from airguns and fin whales recorded in the mid-Atlantic Ocean, 1999–2009, *J. Acoust. Soc. Am.*, *131*, 1102–1112, doi:10.1121/1.3672648.

Park, M., R. I. Odom, and D. J. Soukup (2001), Modal scattering: A key to understanding oceanic T-waves, *Geophys. Res. Lett.*, *28*(17), 3401–3404, doi:10.1029/2001GL013472.

Parks, S. E., C. W. Clark, and P. L. Tyack (2007), Short-and long-term changes in right whale calling behavior: The potential effects of noise on acoustic communication, *J. Acoust. Soc. Am.*, *122*, 3725–3731, doi:10.1121/1.2799904.

Porter, M. B., and Y.-C. Liu (1994), Finite-element ray tracing, in *Theoretical and Computational Acoustics*, vol. 2, pp. 947–956, World Sci., Singapore. [Code and manual available at http://oalib.hlsresearch.com/Rays/index.html.]

Richardson, W. J., C. R. Greene, C. I. Malme, and D. H. Thomson (1995), *Marine Mammals and Noise*, Academic, San Diego, Calif.

Risch, D., P. J. Corkeron, W. T. Ellison, and S. M. Van Parijs (2012), Changes in humpback whale song occurrence in response to an acoustic source 200 km away, *PLoS ONE*, *7*, e29741, doi:10.1371/journal.pone.0029741.

Soto, N. A., M. Johnson, P. T. Madsen, P. L. Tyack, A. Bocconcelli, and J. Fabrizio Borsani (2006), Does intense ship noise disrupt foraging in deep-diving Cuvier's beaked whales (*Ziphius Cavirostris*)?, *Mar. Mamm. Sci.*, *22*, 690–699, doi:10.1111/j.1748-7692.2006.00044.x.

Southall, B. L., et al. (2007), Marine mammal noise exposure criteria: Initial scientific recommendations, *Aquat. Mamm.*, *33*, 411–414, doi:10.1578/AM.33.4.2007.411.

Talandier, J., and E. A. Okal (1998), On the mechanism of conversion of seismic waves to and from T waves in the vicinity of island shores, *Bull. Seismol. Soc. Am.*, *88*, 621–632.

Taylor, B., K. Zellmer, F. Martinez, and A. Goodliffe (1996), Seafloor spreading in the Lau back-arc basin, *Earth Planet. Sci. Lett.*, *144*(1–2), 35–40, doi:10.1016/0012-821X(96)00148-3.

Tolstoy, I., and M. Ewing (1950), The T phase of shallow-focus earthquakes, *Bull. Seismol. Soc. Am.*, *40*, 25–51.

Tolstoy, M., J. Diebold, S. Webb, D. Bohnenstiehl, E. Chapp, R. Holmes, and M. Rawson (2004), Broadband calibration of R/V *Ewing* seismic sources, *Geophys. Res. Lett.*, *31*, L14310, doi:10.1029/2004GL020234.

Tolstoy, M., J. Diebold, L. Doermann, S. Nooner, S. Webb, D. R. Bohnenstiehl, T. Crone, and R. Holmes (2009), Broadband calibration of the R/V *Marcus G. Langseth* four-string seismic sources, *Geochem. Geophys. Geosyst.*, *10*, Q08011, doi:10.1029/2009GC002451.

Urick, R., D. Heiberg, and J. Davis (Eds.) (1983), *Principles of Underwater Sound*, McGraw-Hill, New York.

Vaughan, R. G., and P. W. Webley (2010), Satellite observations of a surtseyan eruption: Hunga Ha'apai, Tonga, *J. Volcanol. Geotherm. Res.*, *198*, 177–186, doi:10.1016/j.jvolgeores.2010.08.017.

Williams, C. M., R. A. Stephen, and D. K. Smith (2006), Hydroacoustic events located at the intersection of the Atlantis (30°N) and Kane (23° 40′N) transform faults with the Mid-Atlantic Ridge, *Geochem. Geophys. Geosyst.*, *7*, Q06015, doi:10.1029/2005GC001127.

Yang, Y., and D. W. Forsyth (2003), Improving epicentral and magnitude estimation of earthquakes from T phases by considering the excitation function, *Bull. Seismol. Soc. Am.*, *93*(5), 2106–2122, doi:10.1785/0120020215.

Young, R. W. (1970), On the energy transported with a sound pulse, *J. Acoust. Soc. Am.*, *47*, 441–442, doi:10.1121/1.1911547.